Synergistic effects of enhanced rock weathering and organic inputs on soil carbon accrual.

Jaeeun Sohng*[1,2], Noah W. Sokol[3], Peter K. Weber[3], Steffen Schweizer[4], Keith Morrison[3], Seth Whiteaker[1], Radomir Schmidt[1], Isabel Montañez[1,5], Anthony O'Geen[2], Kate Scow[2]

Institutional affiliations

[1] University of California, Davis, Institute of the Environment, The Barn, 501 Engineering Bikeway, Davis, California, 95616, USA
[2] University of California, Davis, Department of Land, Air and Water Resources, One Shields Avenue, Davis, California, 95616, USA
[3] Lawrence Livermore National Laboratory, Physical and Life Science Directorate, 7000 East Avenue, Livermore, California, 94550, USA
[4] Technical University of Munich, TUM School of Life Sciences, Chair of Soil Science, Freising, Germany
[5] University of California, Davis, Department of Earth and Planetary Sciences, Academic Surge, 1124 Crocker Ln, Davis, California, 95616, USA

***Corresponding author's contact information**
jsohng@ucdavis.edu

ABSTRACT

Enhanced Rock Weathering (ERW)—the application of crushed silicate minerals to croplands—holds promise for drawing down excess atmospheric carbon dioxide through accelerated biological and chemical weathering. Silicate rock amendments, such as olivine and basalt, are increasingly recognized for increasing inorganic carbon (C) drawdown by enhancing the flux of soil alkalinity. However, their effects on soil organic carbon (SOC)—Earth's largest terrestrial C reservoir and a key driver of soil fertility regulated by microbial processes—remain underexplored, especially when combined with organic amendments commonly used in agriculture to promote organic C accrual and soil health. In a soil microcosm study, we assessed the impact of adding a readily available C source in combination with olivine inputs on soil C and microbial dynamics over a 55-week incubation period. Additionally, we used ^{13}C-glucose tracers to track C flow across early and late incubation stages, and NanoSIMS imaging to directly visualize organic matter-mineral interactions. Co-application of olivine and glucose led to higher total C, greater microbial biomass, lower microbial respiration per unit biomass, and increased mineral-associated organic matter (MAOM) formation with greater incorporation of new C—surpassing the effects of either amendment alone. NanoSIMS imaging and SEM-EDS revealed a microscale distribution of glucose-derived ^{13}C across mineral-dominated and OM-dominated patches that were not directly co-located with olivine particles. Treatments without an organic input showed limited changes in microbial C use strategies or lower SOC. Our findings

provide some of the first direct evidence for synergistic effects of crushed rock and organic inputs on soil C accrual, through microbial processes that enhance both organic and inorganic C storage. Integrating ERW with organic inputs enhances biologically mediated C retention, strengthening both climate mitigation potential and soil health, especially in agroecosystems where microbial functioning is vital yet vulnerable.

Keywords

Enhanced Rock Weathering (ERW)
Olivine
Organic Amendments
Soil Microcosm Incubation
Microbial Metabolic Quotient (qCO_2)
Mineral-Associated Organic Matter (MAOM)
Organo–organic Interactions
Nature-Based Carbon Removal

1. Introduction

There is an urgent need to remove up to ten gigatonnes of carbon dioxide (CO_2) per year from the atmosphere to stabilize global climate (National Academies of Sciences, Engineering, and Medicine, 2019). Enhanced Rock Weathering (ERW) has gained traction as a promising CO_2 removal approach, given its potential for wide scale deployment on agricultural lands and the range of co-benefits it offers for soil health, pH, water and nutrient management, reduced trace gas emissions, and crop yields (Beerling et al., 2020; Haque et al., 2020; Holzer et al., 2023; Beerling et al., 2024). The application of crushed silicate rocks to soils accelerates chemical weathering, which effectively draws CO_2 from the atmosphere and converts it into dissolved inorganic carbon (C) species (Hartmann et al., 2013; Kantzas et al., 2022). While agricultural lands offer practical advantages for ERW deployment—such as existing spreading infrastructure and water management systems—the effectiveness and outcomes of ERW are soil-type and context dependent, with potential for both co-benefits and unintended effects (e.g., from shifts in alkalinity), underscoring the need for site-specific evaluation.

A major outstanding question with respect to ERW is the effect of crushed rock amendments on soil organic carbon (SOC). SOC is the largest terrestrial pool of organic C, and it is critical for soil health and crop productivity (Mitchell et al., 2017; Crowther et al., 2019). In croplands, ERW is hypothesized to affect SOC because the application of crushed rock alters the physicochemical soil environment—such as increasing soil pH, releasing base cations (e.g., Ca^{2+}, Mg^{2+}), shifting redox conditions, and influencing mineral surface availability—which can directly affect the stabilization of organic matter (OM) on minerals, as well as affect microbial community composition and function (Buss et al., 2024; Corbett et al., 2024; Ramos et al., 2024;

Lei et al., 2025). Even modest shifts in SOC under ERW could have significant implications for net C removal (Smith et al., 2008).

Microbial community dynamics are likely to play a central role in the interplay between ERW and SOC because microbes drive C and nutrient cycling in soil (Kallenbach et al., 2015; Brenzinger et al., 2021; Hartmann and Six, 2023) and mediate mineral weathering and secondary mineral formation (Banfield et al., 1999; Doetterl et al., 2018; Wild et al., 2022) through direct (i.e., mineral dissolution) and indirect (e.g., acidifying their surroundings, exuding organic ligands) influences (Uroz et al., 2022; Wild et al., 2022). Furthermore, SOC is typically sustained through biological practices such as applying organic amendments (e.g., compost), maintaining cover crops, and minimizing tillage—strategies that promote microbial activity and functional diversity and enhance long-term productivity and C persistence (Mitchell et al., 2017; Schmidt et al., 2019; Lehmann et al., 2020; Brenzinger et al., 2021; Shen et al., 2024).

A small number of recent studies examines how ERW influences organic C dynamics and microbial processes (Sokol et al., 2024; Xu et al., 2024; Timmermann et al., 2025). ERW alters soil geochemistry—such as pH, base cation concentrations, and mineral phases—which can affect microbial activity, C turnover, and OM stabilization (Vicca et al., 2021; Lei et al., 2025). Weathering products like poorly crystalline oxy-hydroxides and clays also provide reactive surfaces for binding microbial byproducts and organic compounds (Slessarev et al., 2021; Buss et al., 2024). These biogeochemical interactions can influence both particulate organic matter (POM)—a more labile and microbially accessible pool—and mineral-associated organic matter (MAOM)—the largest and most persistent pool of SOC (Cotrufo et al., 2019; Sokol et al., 2022). ERW may influence MAOM formation and aggregation not only by increasing mineral surface area, but also by altering soil chemistry in ways that affect microbial C utilization, organo-mineral bonding, and stabilization pathways (Dong et al., 2022; Kang et al., 2024). However, these changes may also stimulate microbial decomposition or priming, adding uncertainty to the net balance between C retention and loss (Fang et al., 2023; Yan et al., 2023). Co-applying ERW with organic inputs may strengthen microbe–mineral interactions and supply energy that help microbes adapt to altered geochemical conditions, potentially offsetting metabolic stress and enhancing SOC stabilization (Schimel, 2007; Corbett et al., 2024; Oladele et al., 2024). These studies highlight ways that ERW, organic C cycling and microbes can interact, but more work is necessary to predict how adding organic compound (e.g. C/energy source) in combination with ERW impacts on SOC and microbial dynamics under agricultural management.

Here, in a controlled 55-week microcosm study, we directly tested how crushed rock (olivine, a silicate mineral used in ERW) interacts with an organic input (glucose, a readily available C and energy source for many soil microbes) by using isotopic tracers and micro-scale imaging to illuminate their effects on soil C dynamics and microbial processes. Over the incubation period, we intensively monitored how olivine weathering interacted with an organic input to affect microbial biomass carbon (MBC), soil respiration, and soil C fractions (MAOM and POM). To

track C flow, we conducted additional 12-week sub-incubations using a single pulse of ^{13}C-labeled glucose on soils collected at early (week 15) and late (week 55) incubation stages, tracking ^{13}C incorporation into MBC, respiration, and C fractions. We hypothesized that co-application of olivine and glucose would: (1) accelerate rock weathering relative to olivine alone, as measured through weathering indicators like increased pH, dissolved inorganic C (IC) concentration, increased cation release and mineral transformations; (2) promote greater MBC while reducing respiration relative to glucose-only treatments; and (3) increase microbially-mediated formation of MAOM compared to glucose-only treatments.

2. Materials and methods

2.1 Experimental design

We conducted long-term laboratory incubations using soil and crushed olivine rock from a paired ERW field study, as described in Holzer et al., 2023 and Sokol et al., 2024. Soil was collected from the UC Davis Campbell Tract Agricultural Research Station in Yolo County, California (38°31'53.96"N, 121°46'54.15"W), which is classified as a fine-silty, mixed, superactive, nonacid, thermic Mollic Xerofluvents, in the Yolo series. The soil texture is silt loam with 14% sand, 61% silt, and 25% clay (Holzer et al., 2023). Samples were collected from the top 10 cm during fall 2022. Bulk density was directly measured from the sampling plots in 2021 from a Geoprobe core sample. Water holding capacity (WHC) for the Yolo series soil was determined to be 0.26 g water/g soil (Zárate-Valdez et al., 2006). Post-collection, soil was passed through a 4 mm mesh to ensure homogeneity and stored under controlled conditions at 4°C with breathable lids to maintain necessary aeration.

Long-term laboratory microcosm incubations (Figure 1a) included six treatments: a control (no olivine or glucose), Olivine3% (3% by dry mass), Olivine10% (10% by dry mass), Glucose-only (Glucose), Olivine3%+Glucose, and Olivine10%+Glucose. The olivine was a mining byproduct (Rock Dust Local, Bridport, VT) and consisted of 87% olivine by weight, as determined by QEMSCAN Bulk Mineral Analysis (Holzer et al., 2023). Quantitative X-ray Diffraction (QXRD) further confirmed that 85% of the crystalline fraction was forsterite, the magnesium-rich endmember of the olivine group (Table S1). The particle size distribution was 25% <2 μm, 62% between 2–53 μm, and 10% between 53–200 μm (Table S2).

Olivine application rates were determined based on soil dry mass (i.e., 3% olivine mass = olivine / [olivine + soil mass]), with 3% and 10% olivine corresponding to field application rates of 40 tonnes/ha and 132 tonnes/ha, respectively, assuming a 10 cm soil depth and a bulk density of 1.32 g/cm³. For microcosm preparation, 200 g of soil were placed in 1-quart glass jars and pre-incubated at 50% WHC (0.13 g/g) in the dark at 20.5°C for six days. Following pre-incubation, olivine powder was thoroughly mixed into the soil, ensuring uniform distribution and break-down of large aggregates.

Each treatment was replicated four times across four destructive harvests at 15, 30, and 55 weeks (Figure 1a), with an additional control set—without multi-nutrient supplement—harvested at 55 weeks. A total of 96 microcosm jars were maintained at 20.5°C and 70% WHC (0.18 g/g) throughout the incubation period without physical disturbance. Glucose-treated microcosms received 1.75 mg of glucose per gram of dry soil every three weeks (0.7 mg C per g dry soil), totaling 12.6 mg C per gram by the end of the experiment (Kallenbach et al., 2016). The non-glucose treatments received the same volume of deionized water in place of glucose solution at the same time intervals.

C parameters (total C [TC], [POM], and [MAOM]) were measured over time. Values at each harvest were baseline-corrected by subtracting the initial concentrations measured from a separate set of Time 0 jars (post-amendment). These baseline-adjusted values are reported as delta (Δ) values throughout the manuscript (e.g., ΔTC and ΔMAOM).

All microcosms, except the control set, received three additional inputs of a stoichiometrically balanced multi-nutrient solution every 15 weeks (C:N:P:S:K = 10000:833:200:143:252) (Kirkby et al., 2013). Each addition provided 0.408 mg N, 0.098 mg P, 0.07 mg S, and 0.124 mg K per gram of dry soil, with total additions over 55 weeks amounting to 1.22 mg N, 0.29 mg P, 0.21 mg S, and 0.37 mg K per gram. The solution consisted of ammonium nitrate (NH_4NO_3), ammonium sulfate ($(NH_4)_2SO_4$), and potassium dihydrogen phosphate (KH_2PO_4), adjusted to pH 7 using 10 M sodium hydroxide (NaOH).

2.2 Soil and carbon fraction analysis

During incubation, jars were covered with perforated lids to allow air exchange. To monitor microbial respiration, the jars were sealed with airtight lids equipped with a septum for 24 hours to facilitate headspace gas measurement using an infrared gas analyzer (IRGA, LiCOR Biosciences; Li850; Slessarev et al., 2020). Soil respiration rates (μg C hr^{-1} g^{-1} soil) were recorded weekly for the initial 40 weeks and every three weeks thereafter until week 55.

At the initial time point (Time 0) and each destructive sampling interval (15, 30, and 55 weeks; Figure 1a), the full 200 g of incubated soil was sieved to 4 mm for homogenization before subsampling for a suite of analyses. Soil IC concentration was obtained by acidifying a subsample in a sealed glass jar with 10 mL of 1M phosphoric acid (H_3PO_4), and the evolved CO_2 was quantified using an IRGA. MBC was measured by fumigating 6 g of fresh soil with chloroform under vacuum in darkness for 24 hours. Post-fumigation, both fumigated and non-fumigated samples were extracted with 30 mL of 1 M K_2SO_4 and analyzed for dissolved organic C via UV-persulfate digestion (Teledyne Fusion), with MBC calculated as the difference between fumigated and non-fumigated samples.

Air-dried, 2 mm-sieved soils were used for pH, exchangeable cation, and total carbon (TC) analysis. Soil pH was measured in a 1:2 soil-to-deionized water ratio (Thomas, 1996).

Exchangeable cations (Ca^{2+}, Mg^{2+}, Ni^{2+}, Ba^{2+}, Mn^{2+}, Sr^{2+}, Si^{4+}) were extracted from 2 g of soil using 1 M ammonium acetate at pH 7, filtered through Whatman Q5 filter paper (Gavlak et al., 2005), and analyzed via inductively coupled plasma optical emission spectrometry (ICP-OES; iCAP 7000 Series, Thermo Scientific, Davis, California, USA). TC was measured on bulk soil that was finely ground using a ball mill, analyzed with an elemental analyzer (Costech, Davis, California, USA).

At Time 0 and the final sampling point (week 55), <2 mm-sieved soil was analyzed for POM and MAOM. These fractions were obtained using the two-pool method (Cambardella and Elliott, 1992; Bradford et al., 2008): 5 g of soil was dispersed in 0.5% sodium hexametaphosphate and shaken for 18 hours, then wet-sieved at 53 μm to separate MAOM (<53 μm) from POM (retained). Each fraction was dried at 60°C, ground with a ball mill, and analyzed for C content using an elemental analyzer (Costech, Davis, California, USA). Mass recovery after fractionation averaged 100.76% ± 0.48% (mean ± SD) across all samples from the main incubation and 109.40% ± 7.18% for the ^{13}C-glucose sub-incubation.

2.3 Quantitative X-ray Diffraction (QXRD)

QXRD was conducted at Lawrence Livermore National Laboratory to assess changes in soil mineralogy between Time 0 and week 55 samples (Fossum et al., 2021). Soil samples were first crushed and sieved through a 500-μm mesh. Two grams of soil were then spiked with an internal standard (10 Wt. % Al2O3 99.99%, American Elements) and ground for 5 minutes with 15 mL of methanol using a McCrone mill. A portion of the samples were run with no internal standard to determine if any minor phases were not identified due to dilution from the addition of the internal standard. The ground samples were air-dried on a tray and homogenized for 3 minutes with 10 mm plastic beads using a vortex mixer (Bakker et al., 2018). The samples were side-loaded into XRD sample mounts and analyzed on a Bruker D8 advance XRD, scanning from 3° to 65° 2θ at 0.01° increments with a 5-second per step count time. Quantitative mineralogy was determined using BGMN Rietveld refinement facilitated by the Profex interface software (Doebelin and Kleeberg, 2015). XRD patterns were refined to fit crystal unit cell parameters, size, site occupancy, and preferred orientation.

Additionally, mineral intensity factors (MIF) were calculated for forsterite in the olivine standard using soil samples with varying concentrations of the olivine standard (Zhou et al., 2018). The MIF values were obtained using equation (1), where Ix represents the intensity of the forsterite peak at 32.287° 2θ (2.77 Å), Is represents the intensity of the internal standard Al2O3 peak at 43.349° 2θ (2.09 Å), %S is the Wt. % mass of the internal standard and %X represents the mineral weight percent. Once the MIF values were calculated from the olivine standards, the equation can be rearranged to solve for the mineral weight percent (%X).

$$\text{MIF} = \left(\frac{Ix}{Is}\right)\left(\frac{\%S}{\%X}\right) \qquad \text{Equation (1)}$$

2.4 ^{13}C-glucose sub-incubation and soil carbon fractions

To track microbial C allocation across different C fractions in response to different weathering durations termed short- and long-term weathered olivine, 30 g of soil was subsampled from the 200 g soil incubations at weeks 15 and 55 for separate 12-weeks ^{13}C-glucose incubations (Figure 1b). A single pulse of ^{13}C-labeled glucose substrate ($^{13}C_6H_{12}O_6$, ≥99 atom % ^{13}C, Aldrich) was applied to all six experimental conditions at a rate of 1 mg C per gram of soil. The 30 g soil subsamples were packed into centrifuge tubes to maintain a similar soil depth as the main incubation and were incubated in sealed 1-liter jars under conditions consistent with the long-term incubation (70% of water holding capacity, 20.5°C). To assess cumulative CO_2 respiration, a parallel set of identical jars treated with unlabeled natural abundance (^{12}C) glucose was assembled, along with additional control samples (No-C control) that did not receive any C substrate as a reference for microbial responses in the absence of glucose pulse.

At the end of each incubation, the ^{12}C incubation set was opened for MBC analysis via fumigation. For the ^{13}C incubation set, the ^{13}C-labeled soils were processed to quantify MBC, IC, MAOM, POM, and TC. Samples followed the same processing workflow as the long-term incubation described in Section 2.2. Stable isotope analysis was conducted at the UC Davis Stable Isotope Facility for ^{13}C concentrations in IC, MAOM, POM, and TC, while ^{13}C-MBC measurements were performed at the Yale Analytical and Stable Isotope Center.

The microbial metabolic quotient (*mg CO_2-C/mg MBC/h*) was calculated using microbial respiration rates (*mg CO_2-C/g soil/hour*) and microbial biomass (*mg MBC/g soil*) following Equation (2) (Xu et al., 2017; Risch et al., 2023).

$$\underset{(mg\ CO_2-C/mg\ MBC/h)}{Microbial\ Metabolic\ Quotient} = \frac{Microbial\ respiration\ rate\ (mg\ CO_2-C/g\ soil/hour)}{Microbial\ biomass\ (mg\ MBC/g\ soil)} \qquad Equation\ (2)$$

2.5 ^{13}C labeled MAOM analyzed using advanced imaging techniques

Nano-scale secondary ion mass spectrometry (NanoSIMS)

NanoSIMS imaging was performed using a NanoSIMS 50 instrument (CAMECA, Gennevilliers, France) at Lawrence Livermore National Laboratory to investigate ^{13}C incorporation into MAOM (Figure 1b). Three amended treatments—Olivine10%, Glucose-only, and Olivine10%+Glucose—were selected, along with the control soil included in each session to monitor instrument stability and correct for potential instrumental fractionation effects. The <53 μm MAOM fraction was isolated and deposited onto silicon wafers then sputter coated with Au. Samples were scanned (rasterized) with a resolution of 256 x 256 pixels using a Cs^+ primary ion beam at a beam current of 2 pA with a dwell time of 1 ms pixel^{-1}. The secondary ions monitored during scanning were $^{12}C_2^-$, $^{13}C^{12}C^-$, $^{12}C^{14}N^-$, $^{13}C^{14}N^-$, and $^{31}P^-$. Secondary electrons (SE) were monitored for sample visualization. The secondary mass spectrometer was tuned to ~7000 mass

resolution (Pett-Ridge and Weber, 2022) to distinguish mass isobars (e.g., $^{13}C^-$ versus $^{12}C^1H^-$). High-resolution isotopic mapping was performed with a 30-µm field of view: 31 images for the untreated soil (control), 25 for Olivine10%, 24 for Glucose-only, and 31 images for Olivine10%+Glucose.

The data was pre-processed including dead-time correction and co-alignment using NanoT (Hu et al., 2024). A supervised segmentation approach based on a machine-learning algorithm was applied to differentiate mineral-dominated and OM-dominated regions in combination with ^{13}C hotspots (Schweizer et al., 2018; Wilhelm et al., 2022). This enabled a pixel-based identification of non-enriched native OM (high counts for C and N species), native OM associated with the amended ^{13}C-enriched substrate (OM co-located ^{13}C), mineral-dominated surfaces (high SE counts), and mineral-dominated surfaces exhibiting ^{13}C-enrichment from the substrate (high SE and ^{13}C counts; Figure S4 and Figure S5). Quantitative analysis of ^{13}C enrichment was performed by assessing the co-location of enriched ^{13}C spots with mineral and OM-dominated surfaces. For accurate visualization, the ^{13}C enrichment ratios were corrected for the measured cluster ions with ^{12}C according to Shabtai et al. (2024).

Scanning electron microscopy with energy-dispersive X-ray spectroscopy (SEM-EDS)

The regions within the <53 µm MAOM fractions that were analyzed by NanoSIMS were mapped for Mg, Al and Fe by SEM-EDS using an FEI Inspect F SEM equipped with a Bruker Quantax EDS system with an XFlash® silicon drift detector. Secondary electrons were imaged for sample visualization. The analysis electron beam energy was 15 keV. The data were processed using ESPRIT software to generate qualitative elemental maps, which visualize the relative distribution and intensity of element-specific signals derived from EDS measurements. The SEM-EDS data were super-positioned on the NanoSIMS measurements by translation and rotation of the images to identify Mg-rich olivine particles. The maps were correlated with the NanoSIMS data based on the marks left by the NanoSIMS sputtering visible in the SEM.

2.6 Statistical and data analysis

Statistical analyses and data visualization were performed using R version 4.4.0 (R Core Team, 2024). Linear regression models were fit using the factors ‘Treatment’ and ‘Time’ with the base R stats package. For models incorporating the interaction between ‘Treatment’ and ‘Time,’ a two-way analysis of variance (ANOVA) was conducted. One-way ANOVA was used for models assessing treatment differences in soil chemistry and C pool concentrations where time was not a factor. Pairwise comparisons between treatments within one sampling point were made using Tukey’s HSD, with letters indicating significance, as implemented in the *emmeans* package. Residuals were examined for normality and homogeneity of variance to ensure the validity of our analyses. Normality was assessed using the Shapiro-Wilk test and visualized with QQ-plots from the *DHARMa* package (Hartig, 2022). When normality and homogeneity of variance were violated, log-transformations were applied. Statistical significance was set at $p < 0.05$, with

marginal significance considered (i.e., $0.05 < p < 0.1$). All reported errors represent the standard error of the mean (1 SE).

3. Results

3.1 Soil carbon dynamics

Soils co-amended with glucose and crushed olivine (olivine 10%) exhibited the largest net C increase over time (Figure 2a). Overall, relative to non-glucose treated soils, glucose-treated soils showed a higher ΔTC throughout the 55-week incubation (Figure 2a). The ΔTC increased steadily in both the glucose-only and Olivine3%+Glucose treatments until week 30, after which it declined. In contrast, ΔTC in the Olivine10%+Glucose treatment continued to rise throughout the full incubation period, resulting in the highest net C gain by week 55. Non-glucose treatments (Control, Olivine3%, and Olivine10%) showed consistently lower ΔTC values. These remained relatively stable until week 30, followed by a notable decline between weeks 30 - 55.

MBC increased substantially with glucose addition, with the greatest increase observed in the highest olivine dose (olivine 10%) (Figure 2b). Olivine, glucose and their interaction significantly influenced MBC over time (Figure 2b). Across the 55-week incubation, MBC remained consistently elevated in glucose-amended soils, increasing steadily from an initial value (318 ± 3 μg C g^{-1} soil) to the highest peak in the Olivine10%+Glucose treatment (1221 ± 37 μg C g^{-1} soil). In contrast, MBC in non-glucose treatments remained relatively stable through week 30, followed by a pronounced decline by week 55. The lowest MBC was observed in the Olivine10% treatment (118 ± 9 μg C g^{-1}; Table S3).

Glucose addition enhanced MAOM accrual and prevented POM losses, while non-glucose treatments exhibited overall declines in POM. ΔMAOM-C increased significantly in glucose-amended soils, with net gains of approximately 1.5–2 mg C g^{-1} soil by week 55 (Figure 2c). Olivine10%+Glucose trended towards a slightly greater increase in MAOM-C ($p < 0.001$). POM-C remained near baseline levels in all glucose treatments, whereas non-glucose treatments exhibited substantial declines in POM-C over time ($p = 0.005$), with ΔPOM-C values falling below baseline by the end of the incubation (Figure 2d).

Soil respiration rates were strongly stimulated by glucose addition, especially during the early incubation period – i.e. weeks 1-2 (Figure S1). Within glucose treatments, olivine content had little influence on respiration dynamics, though Olivine3%+Glucose exhibited slightly elevated rates by week 55. In contrast, respiration rate remained consistently low in all non-glucose treatments, regardless of olivine level.

3.2 ^{13}C-glucose sub-incubations at weeks 15 and 55

^{13}C-glucose incubations (Figure 1b) of week 15 soil revealed that during early stages of weathering olivine—even when paired with glucose—reduced MBC and increased CO_2 respiration (Figure S2a). MBC declined with increasing olivine content, reaching a minimum in the Olivine10%+Glucose group (536 ± 18 μg C g^{-1} soil; Table S4). ^{13}C incorporation into MBC (i.e.^{13}C-MBC) similarly decreased with higher olivine content (Figure S2b), and the Olivine10%+Glucose treatment showed the highest microbial metabolic quotient, indicating greater respiration per unit biomass (Figure S2c). Neither ΔPOM-C nor ΔMAOM-C showed C accrual relative to baseline values (i.e., baseline-subtracted Δ), although ^{13}C-MAOM incorporation was higher in non-glucose treatments (Figure S3).

The ΔPOM-C and ΔMAOM-C did not show significant increase compared to baseline (baseline-subtracted delta; Δ) though ^{13}C-MAOM incorporation was higher in non-glucose soils (Figure S3). The single pulse of ^{13}C-glucose significantly increased MBC relative to No-C controls (243 ± 8 μg C g^{-1} soil; Table S4). Respiration was elevated in glucose-amended soils, with the Olivine10%+Glucose treatment showing the highest CO_2 release (Figure S2a).

In contrast, ^{13}C-glucose incubation of week 55 soils revealed that co-application of glucose and olivine enhanced MBC and ^{13}C incorporation into MAOM. MBC was positively correlated with olivine content in glucose-treated soils, with the Olivine10%+Glucose treatment showing the highest MBC (1004 ± 36 μg C g^{-1} soil; Table S4). At the same time, Olivine10% treatments produced the lowest CO_2 headspace concentrations, regardless of glucose addition (Figure 3a). The ^{13}C content in MBC scaled proportionally with total MBC (Figure 3b). Notably, the Olivine10%+Glucose treatment showed the lowest microbial metabolic quotient, indicating reduced respiration per unit biomass (Figure 3c).

The ^{13}C pulse on week 55 led to relatively uniform incorporation of new C into the MAOM pool in non-glucose treatments, whereas co-amended soils showed an olivine dose-dependent increase in ^{13}C-MAOM, peaking in the Olivine10%+Glucose treatment (361.1 ± 8.6 μg C g^{-1} soil; Figure 4d; Table S4). Within glucose-amended soils, ^{13}C-POM decreased with increasing olivine content (Figure 4b). At week 55, both ΔPOM-C and ΔMAOM-C increased significantly with glucose addition, while olivine alone showed no consistent effect on total POM or MAOM accrual (Figure 4a, c).

3.3 Microscale ^{13}C distribution in the MAOM fraction by NanoSIMS

NanoSIMS imaging showed a heterogeneous distribution of OM patches and ^{13}C hotspots at the microscale (Figure 5a). Across all treatments, 58% of the detected glucose-derived ^{13}C hotspots were co-localized with mineral-dominated regions and 42% were co-localized with OM-dominated regions, likely native MAOM (Figure 5b, c). In the Olivine10%+Glucose treatment, we found the highest co-location of ^{13}C hotspots with OM-dominated regions (46%), whereas the glucose-only treatment showed the highest co-location of ^{13}C hotspots with mineral-dominated regions (63%) (Figure 5b, c). SEM-EDS was used to allocate Mg-rich particles (likely

representing olivine), which revealed that glucose-derived ^{13}C hotspots were not co-localized with olivine particles (Figure S5).

3.4 Weathering indicators

Quantitative XRD revealed significant decreases in olivine content in the 10% treatments after 55 weeks of incubation (Figure 6a). The crushed rock amendment was composed of 85% forsterite-olivine (Table S1), and in the 10% rock treatments, the initial mineral intensity factor (MIF) confirmed that the amended soil contained 8.5% forsterite-olivine at Time 0 (Figure 6a). By week 55, olivine content had decreased to 6.4% ($p = 0.06$) and 6.2% ($p = 0.05$) in treatments with and without glucose, respectively (Figure 6a), consistent with a significant reduction in the forsterite-to-corundum (Al_2O_3) ratio (Figure S6a).

Soil pH was strongly affected by the interactions of glucose, olivine, and time over the 55-week incubation (Figure 6b). The initial pH of the untreated soil was 6.8, and all treatments except the untreated soil showed a pH increase by week 15, followed by a gradual decline over time. Glucose addition initially raised pH by ~0.5 units in Soil+Glucose and by 0.2–0.3 units in the olivine treatments (Table S5), with the highest pH observed in the Olivine10%+Glucose treatment in week 15 (up to pH 7.9). By week 55, glucose effects had diminished, and pH was primarily determined by olivine content: Olivine3% and Olivine10% maintained higher pH (6.24–6.30 and 6.64–6.74, respectively) than non-olivine treatments (5.59–5.62). Untreated and Soil+Glucose treatments declined from peaks of 6.69 and 7.16 to near 5.6.

IC generally mirrored the pH trend, declining significantly across treatments over the 55-week incubation period (Figure S6b). Initial IC ranged from 25.95 to 26.28 µg C g^{-1} soil. During the first 15-weeks, only the Olivine10%+Glucose treatment showed an increase, reaching 29.75 µg C g^{-1} soil, while other treatments remained near their initial levels (23.66 to 26.58 µg C g^{-1} soil). By week 55, IC had declined in all treatments, with the greatest reduction in the Olivine10% treatment, which dropped by -18.56 µg C g^{-1} soil to a final value of 7.47 µg C g^{-1} soil. The remaining treatments stabilized between 14.33 and 16.96 µg C g^{-1} soil (Table S5).

The ^{13}C sub-incubations revealed a significant interaction between olivine and glucose on IC at week 15, but no effect was observed at week 55. At week 15, the Olivine10%+Glucose treatment showed the highest IC concentration (Figure S7a). ^{13}C enrichment in the IC fraction increased with rock content, with both 3% and 10% olivine treatments showing elevated incorporation, and the highest ^{13}C value observed in the Olivine10%+Glucose treatment (Figure 6c). By week 55, IC levels were lowest in the Olivine10% treatments (Figure S7b), and ^{13}C incorporation into IC was minimal across all treatments (Figure S7c).

Olivine amendments significantly increased exchangeable Mg^{2+} and Si^{4+} compared to non-olivine treatments, while glucose co-application had minimal additional effect on these weathering signals (Figure S8). At the final time point, both 3% and 10% olivine treatments

elevated Mg^{2+} and Si^{4+} levels regardless of glucose addition. Notably, Mg^{2+} and Si^{4+} concentrations also increased over time in treatments without olivine.

4. Discussion

4.1 Synergistic effects of olivine and organic inputs on soil C and microbial biomass

In a 55-week enhanced rock weathering (ERW) incubation experiment, we found that co-applying olivine with a readily available organic C source significantly enhanced microbially mediated C cycling and total C (TC) accrual (Figure 2a). Microbial biomass carbon (MBC) followed a similar trajectory, with the olivine–glucose combination supporting greater MBC than glucose alone, particularly toward the end of the 55-week incubation (Figure 2b). This sustained increase suggests that a readily available organic C source intensified microbe–mineral interactions over time, leading to greater allocation of C as mineral-associated organic matter (MAOM) – the largest and slowest cycling pool of soil organic carbon (SOC). Notably, most of the accumulated C was recovered in the MAOM fraction, with minimal gains observed in the faster cycling particulate organic matter (POM) fraction, indicating preferential accumulation of C in the more persistent MAOM fraction (Figures 2c, d).

In contrast, olivine applications alone caused modest changes in TC and MBC which declined significantly after week 30 (Figure 2a, b). This temporal pattern suggests that microbes may increasingly rely on the mineralization of native SOC over time as energy limitations emerge, and thus crushed rock applications may lead to SOC losses unless co-applied with organic substrates (Fang et al., 2023; Schroeder et al., 2024). While olivine's effect on increasing pH and associated nutrient release may create more favorable conditions for micronutrient availability for microbes and plants (Berge et al., 2012; Fang et al., 2023; Skov et al., 2024), it does not supply bioavailable energy to support microbial growth. Indeed, most SOC loss occurred in the more bioavailable POM fraction, while the MAOM fraction remained relatively stable in size over time (Figures 2c, d), consistent with the preferential decomposition of more labile C pools under energy-limited conditions (Cotrufo et al., 2019; Witzgall et al., 2021).

We applied a one-time pulse of isotopically labeled glucose to subsamples of soil collected from the microcosms in order to trace the distribution of newly added C across distinct soil C pools (Figure 1b). Our ^{13}C labeling approach enabled direct tracing of C allocation in early stages (week 15) versus later stages (week 55) of the incubation. At the early stage (week 15), olivine appeared to suppress MBC, even in the presence of glucose, as evidenced by a negative relationship between olivine concentration and ^{13}C assimilation into MBC (Figure S2b). Despite this reduction in biomass, respiratory CO_2 production increased with olivine addition (Figure S2a), indicating a stress response in the microbial community (Xu et al., 2017). Such a response likely redirected energy toward cellular maintenance and respiration rather than growth (Schimel, 2007), consistent with significantly elevated microbial metabolic quotient (qCO_2)—the respiration rate per unit biomass—observed under olivine10%+Glucose (Figure S2c; Risch et al.,

2023). The underlying stress may stem from olivine-induced pH shifts (Figure 6b) or imbalanced nutrient availability, both of which increase microbial metabolic costs and constrain biomass production (Uroz et al., 2009; Min et al., 2021). Collectively, these findings suggest that early-stage olivine weathering imposes physiological stress on soil microbial communities, dampening biomass synthesis and increasing C loss through respiration—even in the presence of a labile C source. This aligns with previous short-term ERW studies that reported elevated C mineralization and reduced SOC, potentially driven by microbial stress responses to rock amendments (Yan et al., 2023; Lei et al., 2025).

Tracing ^{13}C at the later stage of the incubation (week 55), we found that co-application of olivine with glucose increased MBC and newly added ^{13}C incorporation into MBC in proportion to olivine concentration (Figure 3b). Unlike the earlier incubation stage, co-application of olivine and glucose reduced microbial CO_2 respiration and lowered the metabolic quotient compared to the glucose-only treatment (Figures 3a, c), suggesting adaptation to olivine and a shift toward more efficient C utilization. Soils that received regular glucose additions—a readily available C source similar to plant-derived exudates and organic amendments (Reischke et al., 2014)—helped to support MBC, amplifying olivine's positive effects on soil C stabilization. The glucose treatments across a longer timeframe (55 weeks) may have facilitated key microbial community processes such as biofilm formation, nutrient acquisition, and the enrichment of microbial groups adapted to mineral-derived nutrients (Gadd, 2010). Together, olivine and glucose created a favorable environment for sustained microbial growth, likely because the added C source enabled microbes to respond effectively to pH shifts and byproducts release from silicate weathering (Bennett et al., 2001). Interactions may also depend on mineral-surface properties—such as composition, microtopography, surface charge, and hydrophobicity—which influence microbial attachment and community dynamics over time (Dong et al., 2022).

4.2 Synergistic effects of olivine and organic inputs on MAOM formation

The 12-week incubation with a single pulse of ^{13}C-labeled glucose enabled us to trace microbial-derived C that persisted beyond initial metabolic processing—an indicator of SOC stabilization via microbial turnover (Kallenbach et al., 2015). At week 15, glucose-amended treatments exhibited minimal ^{13}C incorporation into both POM and MAOM (Figure S3). By the later stage of the incubation (week 55), however, both fractions significantly increased ^{13}C incorporation in glucose-amended soils (Figure 4a, c), with contrasting trends in ^{13}C allocation. When glucose was supplied as a sustained energy source, ^{13}C incorporation into MAOM increased proportionally with olivine concentration, while ^{13}C-POM declined in the presence of olivine (Figure 4b, d).

This divergence in ^{13}C incorporation into MAOM and POM likely reflects a microbial community shift driven by interactions between olivine weathering and organic inputs. The reduced ^{13}C incorporation into POM under olivine + glucose treatments may indicate altered

microbial activity compared to glucose-only soils—for example, lower fungal biomass or reduced hyphal contributions to POM (Witzgall et al., 2021). Glucose-only treatments showed the lowest ^{13}C incorporation into MAOM (Figure 4d), suggesting that microbial communities—perhaps dominated by fast-growing copiotrophs adapted to high resource availability—channeled a greater share of assimilated C toward respiration rather than biomass production (Fierer et al., 2007; López et al., 2023). In contrast, the pronounced increase in ^{13}C-MAOM under olivine with glucose suggests a shift toward slower-growing, C-conserving microbial taxa better adapted to prolonged weathering and sustained C supply. The decline in microbial metabolic quotient (qCO_2)—respiration per unit biomass—in the Olivine10%+Glucose treatment, from highest at week 15 to lowest at week 55, indicates a shift toward more efficient C utilization (Xu et al., 2017). Non-glucose-treated soils retained higher ^{13}C-MAOM at both earlier and later timepoints (Figure S3d and Figure 4d), likely due to short-lived microbial growth dominated by oligotrophs that efficiently incorporated C into biomass, subsequently contributing to MAOM formation under low-resource conditions (Fierer et al., 2007; Bradford et al., 2008; Mikutta et al., 2019). Collectively, these findings suggest that olivine weathering, when combined with continual inputs of an organic substrate, fosters microbial and geochemical conditions that enhance MAOM formation and long-term SOC stabilization (cf. Wu et al., 2023).

NanoSIMS imaging of ^{13}C hotspots within the MAOM fraction revealed greater ^{13}C association with OM surfaces under olivine + glucose than with either input alone (Figure 5c). The patchy distribution of ^{13}C suggests that microbial residues may act as binding site for new C stabilization, underscoring the importance of microbial assimilation in MAOM formation (Cotrufo et al., 2019; Buckeridge et al., 2020; Mikutta et al., 2019). Notably, glucose-derived ^{13}C hotspots were frequently observed on microstructures lacking elevated Mg signals—a proxy for olivine—suggesting that olivine did not serve as a direct sorbent (Figure S5; Table S1). Instead, our imaging suggests that olivine may have facilitated MAOM formation indirectly by locally altering the physicochemical microenvironment—modifying pH, ionic composition, and nutrient availability—in ways that promoted microbial activity and necromass sorption (Kleber et al., 2021; Dong et al., 2022; Wu et al., 2023). The concurrent increase in MBC suggests that co-applying olivine and glucose sustains microbial populations whose residues may contribute to stable SOM, potentially through hydrophobic interactions between microbial-derived aliphatic compounds (e.g., lipids; Neurath et al., 2021) and pre-existing MAOM (Vogel et al., 2014; Kang et al., 2024).

Our study revealed that co-applying olivine with organic inputs promotes microbially mediated stabilized SOC formation, extending prior work that focused solely on the effects of organic inputs (Kallenbach et al., 2016; Buckeridge et al., 2020; Wasner et al., 2024). While earlier studies have linked microbial processing of OM to the formation of persistent SOC, our findings demonstrate that the addition of reactive minerals can further influence these microbial pathways and contribute to long-term C stabilization. The gradual rise in MAOM by week 55 indicates that

SOC gains from ERW unfold over extended timescales, aligning with field evidence showing C accrual after three or more years (Sokol et al., 2024).

4.3 Coupled effects of olivine and organic input on weathering, pH and inorganic C (IC)

Over the 55-week incubation, olivine weathering progressed significantly, particularly in the Olivine10% treatments. The primary olivine mineral, forsterite, showed a measurable decrease in weight % as measured through QXRD, indicating weathering progression (Figure 6a). While this mineralogical evidence of weathering initially aligned with conventional weathering indicators, pH and IC showed overall decreasing trends, suggesting that processes other than carbonic acid-driven weathering may have occurred. Decoupling between mineral dissolution and carbonate equilibria points to alternative acidification pathways, likely influenced by nutrient solution-derived non-carbonic acids (e.g. via nitrification) (Hasemer et al., 2024). While these multi-nutrient solutions were applied uniformly to support microbial activity, their acidifying effects were significantly buffered in olivine-amended soils.

In addition to increasing TC, and in contrast to olivine-alone treatments, co-applying glucose with olivine enhanced soil pH, particularly in Olivine10%+Glucose. In glucose-amended soils, pH remained elevated by approximately 0.3 units during the first 30 weeks (Figure 6b), likely driven by increased microbial activity and CO_2 release, which promoted greater CO_2 dissolution and carbonic acid formation (Karberg et al., 2005; Reischke et al., 2014). While carbonic acid can be an important source of acidity in slightly acid soils (Karberg et al., 2005; Bargrizan et al., 2020), the buffering capacity of olivine and native mineral surfaces likely buffer the pH in the soil solution by consuming hydronium ions (H_3O^+) and contributing to sustained alkalinity (Ibarra et al., 2016; Xu et al., 2024). A similar pH increase in the glucose-only treatment suggests the native alluvial soil, with its high-surface-area clay-rich minerals, also contributed to pH buffering via surface reactions, thereby sustaining alkalinity (Slessarev et al., 2021).

Beyond C sequestration, ERW may provide co-benefits for agricultural soils through a liming effect. As olivine weathers, it consumes hydrogen ions (H^+) and releases Mg^{2+} and Si^{4+} ions, buffering acidity and increasing soil alkalinity (Renforth et al., 2015; Oelkers et al., 2018). Unlike fast-acting lime, silicate minerals dissolve slowly, offering sustained pH buffering without the CO_2 emissions associated with lime application. This slow-release liming effect can improve nutrient availability and support microbial activity in acid-sensitive soils, such as sandy or weathered tropical soils, though it may also induce large shifts in microbial community composition (Liang et al., 2024). Although our study soils had high base saturation and thus did not require liming, elevated pH in the olivine-amended treatment suggests that ERW can contribute to long-term pH stabilization. These findings support the potential of ERW as a supplementary pH management strategy, particularly in systems where continuous pH stabilization is beneficial. Future research should evaluate its agronomic value under more acidic conditions with high levels of exchangeable acidity (Anda et al., 2015; Paradelo et al., 2015).

Although the decline in IC over time mirrored the pH decrease, we observed a transient IC increase in the Olivine10%+Glucose treatment—from 26 to 29 μg C g^{-1} soil—coinciding with a pH peak at week 15 (Figure S6b). The ^{13}C-glucose pulse experiment confirmed that microbially respired $^{13}CO_2$ was partially fixed into IC, with higher olivine content driving greater ^{13}C incorporation (Figure 6c). This suggests that co-applying olivine with glucose elevated microbially respired CO_2 partial pressure, promoting CO_2 dissolution and alkalinity formation in the presence of weatherable minerals (Vicca et al., 2021; Buss et al., 2024). By week 55, however, IC declined across all treatments (Figure S6b), likely driven by acidification from the multi-nutrient solution and CO_2 degassing as carbonate equilibrium shifted (Hasemer et al., 2024). In agricultural soils, acidity from the ammonia-nitrification based fertilizers may compete with carbonic acids and reduce ERW efficiency in CO_2 removal (Norton and Ouyang, 2019).

This study was conducted in a closed system, where the absence of leaching and gas exchange created distinct soil-solution dynamics. Over time, the accumulation of weathering byproducts and nutrient-derived anions likely altered ionic balances, competed for cation pairing, and reduced carbonate retention, ultimately constraining continued mineral dissolution (Hasemer et al., 2024; Suarez and Skaggs, 2022). In natural systems, bicarbonate remains mobile and can leach from the profile, avoiding CO_2 degassing and supporting continued weathering. Alkalinity may either be exported out of the near field zone or precipitate in the zone as pedogenic carbonate, with outcomes shaped by climate, soil pH, and water flux (Gile et al., 1966; Zamanian et al., 2016; Mills et al., 2024). The experimental constraints of our microcosm study were intentionally imposed, however, to enable precise tracking of C and nutrient transformations, and to isolate the interactions among mineral inputs, organic amendments, and microbial communities. Without such controlled conditions, it would be difficult to generate the mechanistic information needed to advance our understanding of the coupled biogeochemical processes underlying ERW and C stabilization.

5. Conclusion

We directly linked ERW–organic input interactions with MBC dynamics and C accumulation in a controlled microcosm soil system over a year-long timescale and found synergistic effects of co-applying olivine and organic input (glucose) relative to either input alone. We found that co-applying olivine with a readily available C source (glucose) shifted the system from SOC mineralization to accumulation, driven by microbial-mediated C accrual. Olivine initially appeared to stress microbial communities, as indicated by higher respiration rate per unit biomass—highlighting C limitation as a key barrier to ERW efficacy since it may lead to SOC losses. Co-applying olivine and glucose increased TC, MBC, microbial C utilization, and new C incorporation into MAOM—surpassing the effects of either amendment alone. MAOM formation under olivine + glucose was driven more by associations with native OM than by direct sorption of added ^{13}C-glucose to olivine surfaces. This indicates that olivine weathering

contributed indirectly to MAOM formation by biogeochemical interactions and may be decoupled from direct rock surface impacts.

In this context, co-applying labile C is critical for effective ERW deployment. Labile C provides energy that supports microbial resilience and initiates C stabilization pathways (Buckeridge et al., 2020). This is especially relevant in agricultural soils, where amendments such as compost or manure can influence nutrient dynamics and modify weathering outcomes (Oladele et al., 2024). While our study tracked the effects of a specific, highly labile organic input (glucose with nutrient solution), future work should explore how a broader range of organic amendments interact with ERW and influence microbial dynamics. Without sustained bioavailable C, olivine weathering may not shift microbial activity toward SOC retention and may instead trigger microbial mining of native C pools (Figure 2). Although our incubation excluded plant inputs, field systems often include seasonal or continuous labile C sources—such as root exudates—that may alleviate microbial C limitation and amplify ERW efficacy.

Together, these findings suggest that the long-term C sequestration potential of ERW is not solely a geochemical process, but a biogeochemical one—strongly dependent on microbial processes. Our results show that the effectiveness of ERW depends on its integration with organic inputs, mediated by microbial processes that drive weathering, nutrient mobilization, and C stabilization. This study demonstrates that microbial processes are not peripheral but central to ERW outcomes, influencing both inorganic and organic C dynamics. To rigorously evaluate ERW's capacity to contribute to long-term C accumulation, future research must move beyond short-term or mineral-only trials. Long-term field studies are needed that integrate mineral and organic inputs, explicitly account for microbial functionality, and span a range of soil types, climates, and management systems. Such work is essential to determine when and where ERW can be most effective for C management in agricultural landscapes and as a nature-based C removal strategy.

Acknowledgements

This research was supported by the California Strategic Growth Council grant CCR20007. Work at LLNL was supported by the LLNL LDRD Program (22-LW-022; 24-SI-002) and LLNL's 'Terraforming Soil' Energy Earthshot Research Center, funded by the U.S. Department of Energy (award # SCW1841). Work at LLNL was performed under the auspices of the DOE, Contract DE-AC52-07NA27344. N.S., P.W., and S.A.S. were supported by the Bavaria California Technology Center (BaCaTeC) under Project No. 8 [2021-2].

Conflict of Interest

The authors declare no conflicts of interest.

Data Availability Statement

The data that supports the findings of this study are available in the supplementary material of this article.

References

Anda, M., Shamshuddin, J., Fauziah, C.I., 2015. Improving chemical properties of a highly weathered soil using finely ground basalt rocks. CATENA 124, 147–161. https://doi.org/10.1016/j.catena.2014.09.012

Bakker, E., Hubert, F., Wander, M.M., Lanson, B., 2018. Soil Development under Continuous Agriculture at the Morrow Plots Experimental Fields from X-ray Diffraction Profile Modelling. Soil Syst. 2, 46. https://doi.org/10.3390/soilsystems2030046

Banfield, J.F., Barker, W.W., Welch, S.A., Taunton, A., 1999. Biological impact on mineral dissolution: Application of the lichen model to understanding mineral weathering in the rhizosphere. Proc. Natl. Acad. Sci. 96, 3404–3411. https://doi.org/10.1073/pnas.96.7.3404

Bargrizan, S., Smernik, R.J., Mosley, L.M., 2020. Constraining the carbonate system in soils via testing the internal consistency of pH, pCO2 and alkalinity measurements. Geochem. Trans. 21, 4. https://doi.org/10.1186/s12932-020-00069-5

Beerling, D.J., Epihov, D.Z., Kantola, I.B., Masters, M.D., Reershemius, T., Planavsky, N.J., Reinhard, C.T., Jordan, J.S., Thorne, S.J., Weber, J., Val Martin, M., Freckleton, R.P., Hartley, S.E., James, R.H., Pearce, C.R., DeLucia, E.H., Banwart, S.A., 2024. Enhanced weathering in the US Corn Belt delivers carbon removal with agronomic benefits. Proc. Natl. Acad. Sci. 121, e2319436121. https://doi.org/10.1073/pnas.2319436121

Beerling, D.J., Kantzas, E.P., Lomas, M.R., Wade, P., Eufrasio, R.M., Renforth, P., Sarkar, B., Andrews, M.G., James, R.H., Pearce, C.R., Mercure, J.-F., Pollitt, H., Holden, P.B., Edwards, N.R., Khanna, M., Koh, L., Quegan, S., Pidgeon, N.F., Janssens, I.A., Hansen, J., Banwart, S.A., 2020. Potential for large-scale CO2 removal via enhanced rock weathering with croplands. Nature 583, 242–248. https://doi.org/10.1038/s41586-020-2448-9

Bennett, P.C., Rogers, J.R., Choi, W.J., Hiebert, F.K., 2001. Silicates, Silicate Weathering, and Microbial Ecology. Geomicrobiol. J. 18, 3–19. https://doi.org/10.1080/01490450151079734

Berge, H.F.M. ten, Meer, H.G. van der, Steenhuizen, J.W., Goedhart, P.W., Knops, P., Verhagen, J., 2012. Olivine Weathering in Soil, and Its Effects on Growth and Nutrient Uptake in Ryegrass (Lolium perenne L.): A Pot Experiment. PLOS ONE 7, e42098. https://doi.org/10.1371/journal.pone.0042098

Bradford, M.A., Fierer, N., Reynolds, J.F., 2008. Soil carbon stocks in experimental mesocosms are dependent on the rate of labile carbon, nitrogen and phosphorus inputs to soils. Funct. Ecol. 22, 964–974. https://doi.org/10.1111/j.1365-2435.2008.01404.x

Brenzinger, K., Costa, O.Y.A., Ho, A., Koorneef, G., Robroek, B., Molenaar, D., Korthals, G., Bodelier, P.L.E., 2021. Steering microbiomes by organic amendments towards climate-smart agricultural soils. Biol. Fertil. Soils 57, 1053–1074. https://doi.org/10.1007/s00374-021-01599-5

Buckeridge, K.M., Mason, K.E., McNamara, N.P., Ostle, N., Puissant, J., Goodall, T., Griffiths, R.I., Stott, A.W., Whitaker, J., 2020. Environmental and microbial controls on microbial necromass recycling, an important precursor for soil carbon stabilization. Commun. Earth Environ. 1, 36. https://doi.org/10.1038/s43247-020-00031-4

Buss, W., Hasemer, H., Ferguson, S., Borevitz, J., 2024. Stabilisation of soil organic matter with rock dust partially counteracted by plants. Glob. Change Biol. 30, e17052. https://doi.org/10.1111/gcb.17052

Cambardella, C.A., Elliott, E.T., 1992. Particulate Soil Organic-Matter Changes across a Grassland Cultivation Sequence. Soil Sci. Soc. Am. J. 56, 777–783. https://doi.org/10.2136/sssaj1992.03615995005600030017x

Corbett, T.D.W., Westholm, M., Rosling, A., Calogiuri, T., Poetra, R., Niron, H., Hagens, M., Vidal, A., Van Groenigen, J.W., Hartmann, J., Janssens, I.A., Rieder, L., Struyf, E., Van Tendeloo, M., Vlaeminck, S.E., Vicca, S., Neubeck, A., 2024. Organic carbon source controlled microbial olivine dissolution in small-scale

flow-through bioreactors, for CO2 removal. Npj Mater. Degrad. 8, 1–13. https://doi.org/10.1038/s41529-024-00454-w

Cotrufo, M.F., Ranalli, M.G., Haddix, M.L., Six, J., Lugato, E., 2019. Soil carbon storage informed by particulate and mineral-associated organic matter. Nat. Geosci. 12, 989–994. https://doi.org/10.1038/s41561-019-0484-6

Crowther, T.W., van den Hoogen, J., Wan, J., Mayes, M.A., Keiser, A.D., Mo, L., Averill, C., Maynard, D.S., 2019. The global soil community and its influence on biogeochemistry. Science 365, eaav0550. https://doi.org/10.1126/science.aav0550

Doebelin, N., Kleeberg, R., 2015. *Profex* : a graphical user interface for the Rietveld refinement program *BGMN*. J. Appl. Crystallogr. 48, 1573–1580. https://doi.org/10.1107/S1600576715014685

Doetterl, S., Berhe, A.A., Arnold, C., Bodé, S., Fiener, P., Finke, P., Fuchslueger, L., Griepentrog, M., Harden, J.W., Nadeu, E., Schnecker, J., Six, J., Trumbore, S., Van Oost, K., Vogel, C., Boeckx, P., 2018. Links among warming, carbon and microbial dynamics mediated by soil mineral weathering. Nat. Geosci. 11, 589–593. https://doi.org/10.1038/s41561-018-0168-7

Dong, H., Huang, L., Zhao, L., Zeng, Q., Liu, X., Sheng, Y., Shi, L., Wu, G., Jiang, H., Li, F., Zhang, L., Guo, D., Li, G., Hou, W., Chen, H., 2022. A critical review of mineral–microbe interaction and co-evolution: mechanisms and applications. Natl. Sci. Rev. 9, nwac128. https://doi.org/10.1093/nsr/nwac128

Fang, Q., Lu, A., Hong, H., Kuzyakov, Y., Algeo, T.J., Zhao, L., Olshansky, Y., Moravec, B., Barrientes, D.M., Chorover, J., 2023. Mineral weathering is linked to microbial priming in the critical zone. Nat. Commun. 14, 345. https://doi.org/10.1038/s41467-022-35671-x

Fierer, N., Bradford, M.A., Jackson, R.B., 2007. Toward an Ecological Classification of Soil Bacteria. Ecology 88, 1354–1364. https://doi.org/10.1890/05-1839

Fossum, C., Estera-Molina, K., Yuan, M., Herman, D., Chu-Jacoby, I., Nico, P., Morrison, K., Pett-Ridge, J., Firestone, M., 2021. Belowground allocation and dynamics of recently fixed plant carbon in a California annual grassland soil. https://doi.org/10.1101/2021.08.23.457405

Gadd, G.M., 2010. Metals, minerals and microbes: geomicrobiology and bioremediation. Microbiology 156, 609–643. https://doi.org/10.1099/mic.0.037143-0

Gavlak, R., Horneck, D.D., Miller, D.R.O., 2005. Soil, plant and water reference methods for the western region.

Gile, L.H., Peterson, F.F., Grossman, R.B., 1966. MORPHOLOGICAL AND GENETIC SEQUENCES OF CARBONATE ACCUMULATION IN DESERT SOILS. Soil Sci. 101, 347–360.

Haque, F., Santos, R.M., Chiang, Y.W., 2020. Optimizing Inorganic Carbon Sequestration and Crop Yield With Wollastonite Soil Amendment in a Microplot Study. Front. Plant Sci. 11, 1012. https://doi.org/10.3389/fpls.2020.01012

Hartig, F., 2022. DHARMa: residual diagnostics for hierarchical (multi-level/mixed) regression models.

Hartmann, J., West, A.J., Renforth, P., Köhler, P., De La Rocha, C.L., Wolf-Gladrow, D.A., Dürr, H.H., Scheffran, J., 2013. Enhanced chemical weathering as a geoengineering strategy to reduce atmospheric carbon dioxide, supply nutrients, and mitigate ocean acidification. Rev. Geophys. 51, 113–149.

Hartmann, M., Six, J., 2023. Soil structure and microbiome functions in agroecosystems. Nat. Rev. Earth Environ. 4, 4–18. https://doi.org/10.1038/s43017-022-00366-w

Hasemer, H., Borevitz, J., Buss, W., 2024. Measuring enhanced weathering: inorganic carbon-based approaches may be required to complement cation-based approaches. Front. Clim. 6, 1352825. https://doi.org/10.3389/fclim.2024.1352825

Holzer, I.O., Nocco, M.A., Houlton, B.Z., 2023. Direct evidence for atmospheric carbon dioxide removal via enhanced weathering in cropland soil. Environ. Res. Commun. 5, 101004. https://doi.org/10.1088/2515-7620/acfd89

Hu, Y., Zollner, J.M., Höschen, C., Werner, M., Schweizer, S.A., 2024. Automated identification of soil functional components based on NanoSIMS data. Ecol. Inform. 84, 102891. https://doi.org/10.1016/j.ecoinf.2024.102891

Ibarra, D.E., Caves, J.K., Moon, S., Thomas, D.L., Hartmann, J., Chamberlain, C.P., Maher, K., 2016. Differential weathering of basaltic and granitic catchments from concentration–discharge relationships. Geochim. Cosmochim. Acta 190, 265–293. https://doi.org/10.1016/j.gca.2016.07.006

Kallenbach, C.M., Frey, S.D., Grandy, A.S., 2016. Direct evidence for microbial-derived soil organic matter formation and its ecophysiological controls. Nat. Commun. 7, 13630. https://doi.org/10.1038/ncomms13630

Kallenbach, C.M., Grandy, A.S., Frey, S.D., Diefendorf, A.F., 2015. Microbial physiology and necromass regulate agricultural soil carbon accumulation. Soil Biol. Biochem. 91, 279–290. https://doi.org/10.1016/j.soilbio.2015.09.005

Kang, J., Qu, C., Chen, W., Cai, P., Chen, C., Huang, Q., 2024. Organo–organic interactions dominantly drive soil organic carbon accrual. Glob. Change Biol. 30, e17147. https://doi.org/10.1111/gcb.17147

Kantzas, E.P., Val Martin, M., Lomas, M.R., Eufrasio, R.M., Renforth, P., Lewis, A.L., Taylor, L.L., Mecure, J.-F., Pollitt, H., Vercoulen, P.V., Vakilifard, N., Holden, P.B., Edwards, N.R., Koh, L., Pidgeon, N.F., Banwart, S.A., Beerling, D.J., 2022. Substantial carbon drawdown potential from enhanced rock weathering in the United Kingdom. Nat. Geosci. 15, 382–389. https://doi.org/10.1038/s41561-022-00925-2

Karberg, N.J., Pregitzer, K.S., King, J.S., Friend, A.L., Wood, J.R., 2005. Soil carbon dioxide partial pressure and dissolved inorganic carbonate chemistry under elevated carbon dioxide and ozone. Oecologia 142, 296–306. https://doi.org/10.1007/s00442-004-1665-5

Kirkby, C.A., Richardson, A.E., Wade, L.J., Batten, G.D., Blanchard, C., Kirkegaard, J.A., 2013. Carbon-nutrient stoichiometry to increase soil carbon sequestration. Soil Biol. Biochem. 60, 77–86. https://doi.org/10.1016/j.soilbio.2013.01.011

Kleber, M., Bourg, I.C., Coward, E.K., Hansel, C.M., Myneni, S.C.B., Nunan, N., 2021. Dynamic interactions at the mineral–organic matter interface. Nat. Rev. Earth Environ. 2, 402–421. https://doi.org/10.1038/s43017-021-00162-y

Lehmann, J., Hansel, C.M., Kaiser, C., Kleber, M., Maher, K., Manzoni, S., Nunan, N., Reichstein, M., Schimel, J.P., Torn, M.S., Wieder, W.R., Kögel-Knabner, I., 2020. Persistence of soil organic carbon caused by functional complexity. Nat. Geosci. 13, 529–534. https://doi.org/10.1038/s41561-020-0612-3

Lei, K., Bucka, F.B., Teixeira, P.P.C., Buegger, F., Just, C., Kögel-Knabner, I., 2025. Balancing Organic and Inorganic Carbon Dynamics in Enhanced Rock Weathering: Implications for Carbon Sequestration. Glob. Change Biol. 31, e70186. https://doi.org/10.1111/gcb.70186

Liang, Y., Rillig, M.C., Chen, H.Y.H., Shan, R., Ma, Z., 2024. Soil pH drives the relationship between the vertical distribution of soil microbial biomass and soil organic carbon across terrestrial ecosystems: A global synthesis. CATENA 238, 107873. https://doi.org/10.1016/j.catena.2024.107873

López, J.L., Fourie, A., Poppeliers, S.W.M., Pappas, N., Sánchez-Gil, J.J., De Jonge, R., Dutilh, B.E., 2023. Growth rate is a dominant factor predicting the rhizosphere effect. ISME J. 17, 1396–1405. https://doi.org/10.1038/s41396-023-01453-6

Mikutta, R., Turner, S., Schippers, A., Gentsch, N., Meyer-Stüve, S., Condron, L.M., Peltzer, D.A., Richardson, S.J., Eger, A., Hempel, G., Kaiser, K., Klotzbücher, T., Guggenberger, G., 2019. Microbial and abiotic controls on mineral-associated organic matter in soil profiles along an ecosystem gradient. Sci. Rep. 9, 10294. https://doi.org/10.1038/s41598-019-46501-4

Mills, J., Sanchez, J., Olagaray, N., Wang, H., Tune, A., 2024. Foundations for Carbon Dioxide Removal Quantification in ERW Deployments. Cascade Clim.

Min, K., Slessarev, E., Kan, M., McFarlane, K., Oerter, E., Pett-Ridge, J., Nuccio, E., Berhe, A.A., 2021. Active microbial biomass decreases, but microbial growth potential remains similar across soil depth profiles under deeply-vs. shallow-rooted plants. Soil Biol. Biochem. 162, 108401. https://doi.org/10.1016/j.soilbio.2021.108401

Mitchell, J.P., Shrestha, A., Mathesius, K., Scow, K.M., Southard, R.J., Haney, R.L., Schmidt, R., Munk, D.S., Horwath, W.R., 2017. Cover cropping and no-tillage improve soil health in an arid irrigated cropping

system in California's San Joaquin Valley, USA. Soil Tillage Res. 165, 325–335. https://doi.org/10.1016/j.still.2016.09.001

National Academies of Sciences, Engineering, and Medicine, 2019. Negative Emissions Technologies and Reliable Sequestration: A Research Agenda. The National Academies Press, Washington, DC.

Neurath, R.A., Pett-Ridge, J., Chu-Jacoby, I., Herman, D., Whitman, T., Nico, P.S., Lipton, A.S., Kyle, J., Tfaily, M.M., Thompson, A., Firestone, M.K., 2021. Root Carbon Interaction with Soil Minerals Is Dynamic, Leaving a Legacy of Microbially Derived Residues. Environ. Sci. Technol. 55, 13345–13355. https://doi.org/10.1021/acs.est.1c00300

Norton, J., Ouyang, Y., 2019. Controls and Adaptive Management of Nitrification in Agricultural Soils. Front. Microbiol. 10. https://doi.org/10.3389/fmicb.2019.01931

Oelkers, E.H., Declercq, J., Saldi, G.D., Gislason, S.R., Schott, J., 2018. Olivine dissolution rates: A critical review. Chem. Geol. 500, 1–19. https://doi.org/10.1016/j.chemgeo.2018.10.008

Oladele, S.O., Curaqueo, G., Awodun, M.A., 2024. Co-amendment of silicate dust and manure improves soil health metrics and crop yield in coarser-textured more than medium-textured soils. Geoderma Reg. 39, e00887. https://doi.org/10.1016/j.geodrs.2024.e00887

Paradelo, R., Virto, I., Chenu, C., 2015. Net effect of liming on soil organic carbon stocks: A review. Agric. Ecosyst. Environ. 202, 98–107. https://doi.org/10.1016/j.agee.2015.01.005

Pett-Ridge, J., Weber, P.K., 2022. NanoSIP: NanoSIMS Applications for Microbial Biology, in: Navid, A. (Ed.), Microbial Systems Biology: Methods and Protocols. Springer US, New York, NY, pp. 91–136. https://doi.org/10.1007/978-1-0716-1585-0_6

R Core Team, 2024. R: A Language and Environment for Statistical Computing. R Foundation for Statistical Computing, Vienna, Austria. [WWW Document]. URL https://www.r-project.org/ (accessed 9.2.24).

Ramos, E.J., Larsen, W.J., Hou, Y., Muñoz, S., Kemeny, P.C., Scheingross, J.S., Repasch, M.N., Hovius, N., Sachse, D., Ibarra, D.E., Torres, M.A., 2024. Competition or collaboration: Clay formation sets the relationship between silicate weathering and organic carbon burial in soil. Earth Planet. Sci. Lett. 628, 118584. https://doi.org/10.1016/j.epsl.2024.118584

Reischke, S., Rousk, J., Bååth, E., 2014. The effects of glucose loading rates on bacterial and fungal growth in soil. Soil Biol. Biochem. 70, 88–95. https://doi.org/10.1016/j.soilbio.2013.12.011

Renforth, P., Pogge von Strandmann, P.A.E., Henderson, G.M., 2015. The dissolution of olivine added to soil: Implications for enhanced weathering. Appl. Geochem. 61, 109–118. https://doi.org/10.1016/j.apgeochem.2015.05.016

Risch, A.C., Zimmermann, S., Schütz, M., Borer, E.T., Broadbent, A. a. D., Caldeira, M.C., Davies, K.F., Eisenhauer, N., Eskelinen, A., Fay, P.A., Hagedorn, F., Knops, J.M.H., Lembrechts, J.J., MacDougall, A.S., McCulley, R.L., Melbourne, B.A., Moore, J.L., Power, S.A., Seabloom, E.W., Silviera, M.L., Virtanen, R., Yahdjian, L., Ochoa-Hueso, R., 2023. Drivers of the microbial metabolic quotient across global grasslands. Glob. Ecol. Biogeogr. 32, 904–918. https://doi.org/10.1111/geb.13664

Schimel, J., 2007. 18 - SOIL MICROBIOLOGY, ECOLOGY, AND BIOCHEMISTRY FOR THE 21ST CENTURY, in: Paul, E.A. (Ed.), Soil Microbiology, Ecology and Biochemistry (Third Edition). Academic Press, San Diego, pp. 503–514. https://doi.org/10.1016/B978-0-08-047514-1.50022-6

Schmidt, R., Mitchell, J., Scow, K., 2019. Cover cropping and no-till increase diversity and symbiotroph:saprotroph ratios of soil fungal communities. Soil Biol. Biochem. 129, 99–109. https://doi.org/10.1016/j.soilbio.2018.11.010

Schroeder, J., Dămătîrcă, C., Bölscher, T., Chenu, C., Elsgaard, L., Tebbe, C.C., Skadell, L., Poeplau, C., 2024. Liming effects on microbial carbon use efficiency and its potential consequences for soil organic carbon stocks. Soil Biol. Biochem. 191, 109342. https://doi.org/10.1016/j.soilbio.2024.109342

Schweizer, S.A., Hoeschen, C., Schlüter, S., Kögel-Knabner, I., Mueller, C.W., 2018. Rapid soil formation after glacial retreat shaped by spatial patterns of organic matter accrual in microaggregates. Glob. Change Biol. 24, 1637–1650. https://doi.org/10.1111/gcb.14014

Shabtai, I.A., Hafner, B.D., Schweizer, S.A., Höschen, C., Possinger, A., Lehmann, J., Bauerle, T., 2024. Root exudates simultaneously form and disrupt soil organo-mineral associations. Commun. Earth Environ. 5, 699. https://doi.org/10.1038/s43247-024-01879-6

Shen, Y., Zhang, R., Yang, Q., Liu, Z., Li, G., Han, H., Kuzyakov, Y., Ning, T., 2024. Long-term subsoiling and tillage rotation increase carbon storage in soil aggregates and the abundance of autotrophs. Appl. Soil Ecol. 200, 105444. https://doi.org/10.1016/j.apsoil.2024.105444

Skov, K., Wardman, J., Healey, M., McBride, A., Bierowiec, T., Cooper, J., Edeh, I., George, D., Kelland, M.E., Mann, J., Manning, D., Murphy, M.J., Pape, R., Teh, Y.A., Turner, W., Wade, P., Liu, X., 2024. Initial agronomic benefits of enhanced weathering using basalt: A study of spring oat in a temperate climate. PLOS ONE 19, e0295031. https://doi.org/10.1371/journal.pone.0295031

Slessarev, E.W., Chadwick, O.A., Sokol, N.W., Nuccio, E.E., Pett-Ridge, J., 2021. Rock weathering controls the potential for soil carbon storage at a continental scale. Biogeochemistry 157, 1–13. https://doi.org/10.1007/s10533-021-00859-8

Slessarev, E.W., Lin, Y., Jiménez, B.Y., Homyak, P.M., Chadwick, O.A., D'Antonio, C.M., Schimel, J.P., 2020. Cellular and extracellular C contributions to respiration after wetting dry soil. Biogeochemistry 147, 307–324. https://doi.org/10.1007/s10533-020-00645-y

Smith, P., Fang, C., Dawson, J.J.C., Moncrieff, J.B., 2008. Impact of Global Warming on Soil Organic Carbon, in: Advances in Agronomy. Academic Press, pp. 1–43. https://doi.org/10.1016/S0065-2113(07)00001-6

Sokol, N.W., Sohng, J., Moreland, K., Slessarev, E., Goertzen, H., Schmidt, R., Samaddar, S., Holzer, I., Almaraz, M., Geoghegan, E., Houlton, B., Montañez, I., Pett-Ridge, J., Scow, K., 2024. Reduced accrual of mineral-associated organic matter after two years of enhanced rock weathering in cropland soils, though no net losses of soil organic carbon. Biogeochemistry 167, 989–1005. https://doi.org/10.1007/s10533-024-01160-0

Sokol, N.W., Whalen, E.D., Jilling, A., Kallenbach, C., Pett-Ridge, J., Georgiou, K., 2022. Global distribution, formation and fate of mineral-associated soil organic matter under a changing climate: A trait-based perspective. Funct. Ecol. 36, 1411–1429. https://doi.org/10.1111/1365-2435.14040

Suarez, D.L., Skaggs, T.H., 2022. Equilibrium Soil Chemistry Submodels, in: Modeling Processes and Their Interactions in Cropping Systems. John Wiley & Sons, Ltd, pp. 179–201. https://doi.org/10.1002/9780891183860.ch6

Thomas, G.W., 1996. Soil pH and Soil Acidity, in: Methods of Soil Analysis. John Wiley & Sons, Ltd, pp. 475–490. https://doi.org/10.2136/sssabookser5.3.c16

Timmermann, T., Yip, C., Yang, Y., Wemmer, K.A., Chowdhury, A., Dores, D., Takayama, T., Nademanee, S., Traag, B.A., Zamanian, K., González, B., Breecker, D.O., Fierer, N., Slessarev, E.W., Fuenzalida-Meriz, G.A., 2025. Harnessing Microbes to Weather Native Silicates in Agricultural Soils for Scalable Carbon Dioxide Removal. Glob. Change Biol. 31, e70216. https://doi.org/10.1111/gcb.70216

Uroz, S., Calvaruso, C., Turpault, M.-P., Frey-Klett, P., 2009. Mineral weathering by bacteria: ecology, actors and mechanisms. Trends Microbiol. 17, 378–387. https://doi.org/10.1016/j.tim.2009.05.004

Uroz, S., Picard, L., Turpault, M.-P., 2022. Recent progress in understanding the ecology and molecular genetics of soil mineral weathering bacteria. Trends Microbiol. 30, 882–897. https://doi.org/10.1016/j.tim.2022.01.019

Vicca, S., Goll, D.S., Hagens, M., Hartmann, J., Janssens, I.A., Neubeck, A., Peñuelas, J., Poblador, S., Rijnders, J., Sardans, J., Struyf, E., Swoboda, P., van Groenigen, J.W., Vienne, A., Verbruggen, E., 2021. Is the climate change mitigation effect of enhanced silicate weathering governed by biological processes? Glob. Change Biol. 28, 711–726. https://doi.org/10.1111/gcb.15993

Vogel, C., Mueller, C.W., Höschen, C., Buegger, F., Heister, K., Schulz, S., Schloter, M., Kögel-Knabner, I., 2014. Submicron structures provide preferential spots for carbon and nitrogen sequestration in soils. Nat. Commun. 5, 2947. https://doi.org/10.1038/ncomms3947

Wasner, D., Abramoff, R., Griepentrog, M., Venegas, E.Z., Boeckx, P., Doetterl, S., 2024. The Role of Climate, Mineralogy and Stable Aggregates for Soil Organic Carbon Dynamics Along a Geoclimatic Gradient. Glob. Biogeochem. Cycles 38, e2023GB007934. https://doi.org/10.1029/2023GB007934

Wild, B., Gerrits, R., Bonneville, S., 2022. The contribution of living organisms to rock weathering in the critical zone. Npj Mater. Degrad. 6, 1–16. https://doi.org/10.1038/s41529-022-00312-7

Wilhelm, R.C., Lynch, L., Webster, T.M., Schweizer, S., Inagaki, T.M., Tfaily, M.M., Kukkadapu, R., Hoeschen, C., Buckley, D.H., Lehmann, J., 2022. Susceptibility of new soil organic carbon to mineralization during dry-wet cycling in soils from contrasting ends of a precipitation gradient. Soil Biol. Biochem. 169, 108681. https://doi.org/10.1016/j.soilbio.2022.108681

Witzgall, K., Vidal, A., Schubert, D.I., Höschen, C., Schweizer, S.A., Buegger, F., Pouteau, V., Chenu, C., Mueller, C.W., 2021. Particulate organic matter as a functional soil component for persistent soil organic carbon. Nat. Commun. 12, 4115. https://doi.org/10.1038/s41467-021-24192-8

Wu, S., Konhauser, K.O., Chen, B., Huang, L., 2023. "Reactive Mineral Sink" drives soil organic matter dynamics and stabilization. Npj Mater. Sustain. 1, 1–12. https://doi.org/10.1038/s44296-023-00003-7

Xu, T., Yuan, Z., Vicca, S., Goll, D.S., Li, G., Lin, L., Chen, H., Bi, B., Chen, Q., Li, C., Wang, X., Wang, C., Hao, Z., Fang, Y., Beerling, D.J., 2024. Enhanced silicate weathering accelerates forest carbon sequestration by stimulating the soil mineral carbon pump. Glob. Change Biol. 30, e17464. https://doi.org/10.1111/gcb.17464

Xu, X., Schimel, J.P., Janssens, I.A., Song, X., Song, C., Yu, G., Sinsabaugh, R.L., Tang, D., Zhang, X., Thornton, Peter.E., 2017. Global pattern and controls of soil microbial metabolic quotient. Ecol. Monogr. 87, 429–441. https://doi.org/10.1002/ecm.1258

Yan, Y., Dong, X., Li, R., Zhang, Y., Yan, S., Guan, X., Yang, Q., Chen, L., Fang, Y., Zhang, W., Wang, S., 2023. Wollastonite addition stimulates soil organic carbon mineralization: Evidences from 12 land-use types in subtropical China. CATENA 225, 107031. https://doi.org/10.1016/j.catena.2023.107031

Zamanian, K., Pustovoytov, K., Kuzyakov, Y., 2016. Pedogenic carbonates: Forms and formation processes. Earth-Sci. Rev. 157, 1–17. https://doi.org/10.1016/j.earscirev.2016.03.003

Zárate-Valdez, J.L., Zasoski, R.J., Läuchli, A.E., 2006. Short-term effects of moisture content on soil solution pH and soil Eh. Soil Sci. 171, 423. https://doi.org/10.1097/01.ss.0000222887.13383.08

Zhou, X., Liu, D., Bu, H., Deng, L., Liu, H., Yuan, P., Du, P., Song, H., 2018. XRD-based quantitative analysis of clay minerals using reference intensity ratios, mineral intensity factors, Rietveld, and full pattern summation methods: A critical review. Solid Earth Sci. 3, 16–29. https://doi.org/10.1016/j.sesci.2017.12.002

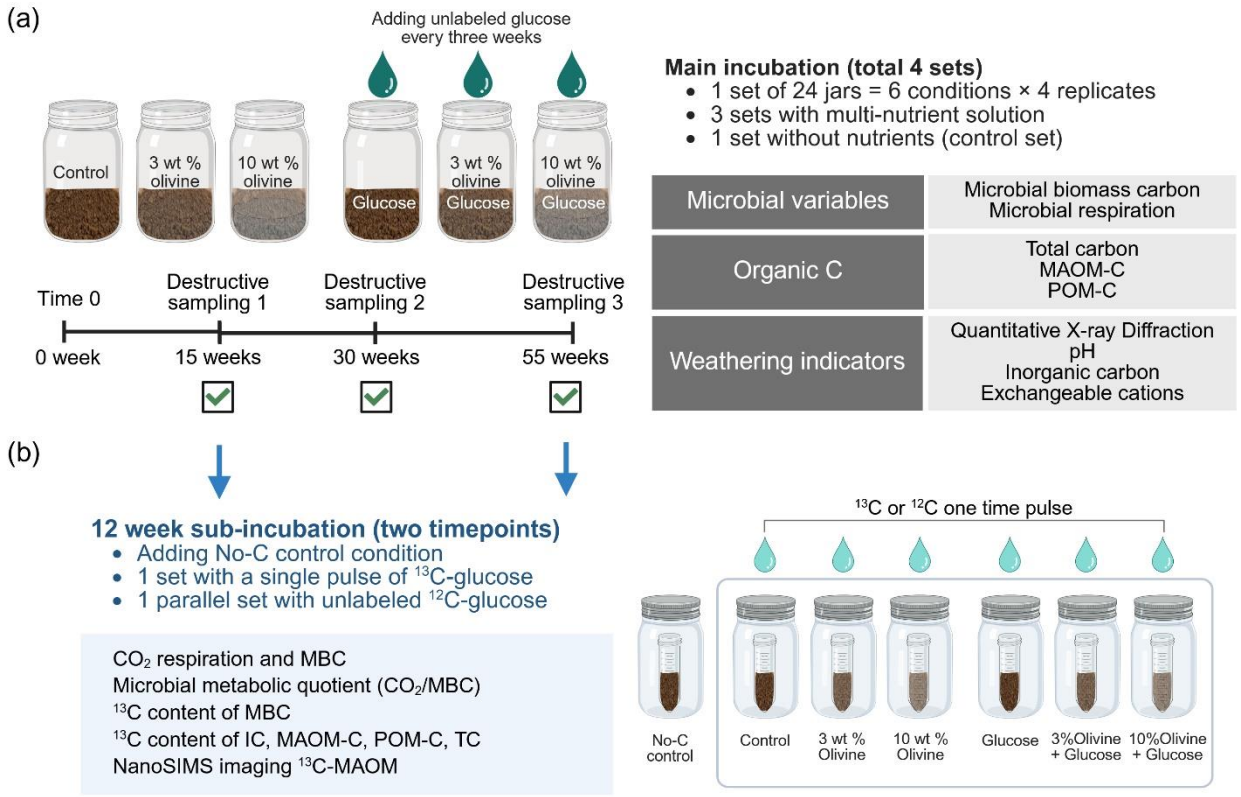

Figure 1. Experimental design and sampling approach of enhanced rock weathering and organic input microcosm study. (a) Schematic of the 55-week soil incubation experiment under six treatments: a control (no olivine or glucose), Olivine3% (3% by dry mass), Olivine10% (10% by dry mass), Glucose-only (Glucose), Olivine3%+Glucose, and Olivine10%+Glucose. Microcosms were destructively sampled at weeks 15, 30, and 55 to assess weathering indicators (e.g., pH, IC, exchangeable cations), microbial responses (respiration, biomass), and carbon fractions (TC, MAOM-C, POM-C). (b) Timeline of 12-week sub-incubation using soil samples collected at weeks 15 and 55. A control (No-C control) condition—without the one-time pulse of labeled or unlabeled glucose—was included. All remaining treatments received a single pulse of either ^{13}C-labeled glucose or unlabeled glucose. Measurements included ^{13}C incorporation into microbial biomass, inorganic and organic carbon fractions, and NanoSIMS imaging of ^{13}C in MAOM.

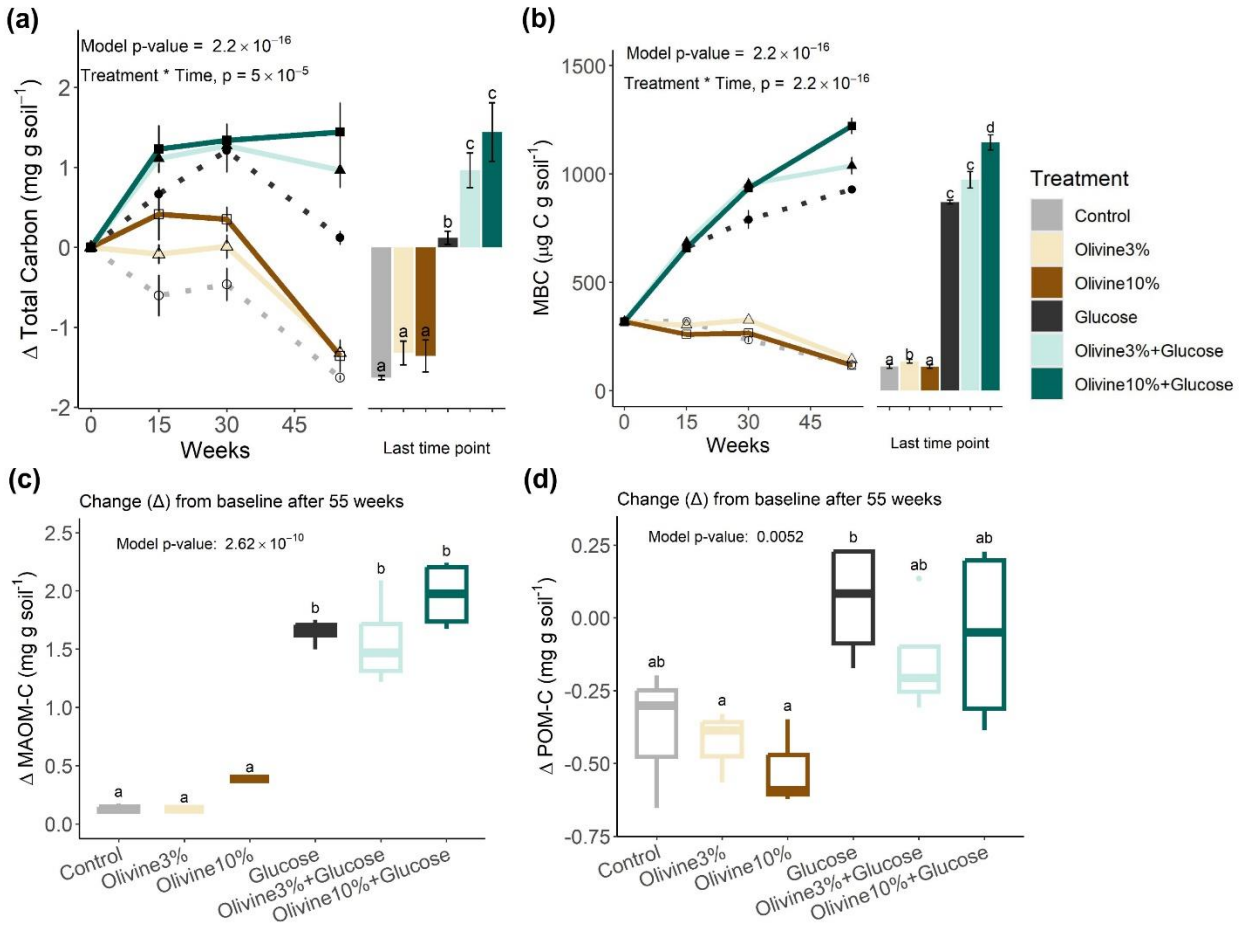

Figure 2. Changes in soil carbon fractions over a 55-week enhanced rock weathering incubation. The study includes six treatments: a control (no olivine or glucose), Olivine3% (3% by dry mass), Olivine10% (10% by dry mass), Glucose-only (Glucose), Olivine3%+Glucose, and Olivine10%+Glucose. (a) Total carbon (Δ; baseline-subtracted; mg C g^{-1} soil). (b) Microbial biomass carbon (MBC; µg C g^{-1} soil). (c) Mineral-associated organic carbon (Δ MAOM-C; mg C g^{-1} soil). (d) Particulate organic matter (Δ POM-C; mg C g^{-1} soil). Statistical significance across treatments (a-b) was assessed using a linear model with treatment and time as fixed effects, reporting the overall model p-value and interaction terms. Bar and box graphs for final time points indicate significant differences among treatments, determined by one-way ANOVA followed by Tukey's post hoc test ($p < 0.05$). Treatments sharing the same letter are not significantly different.

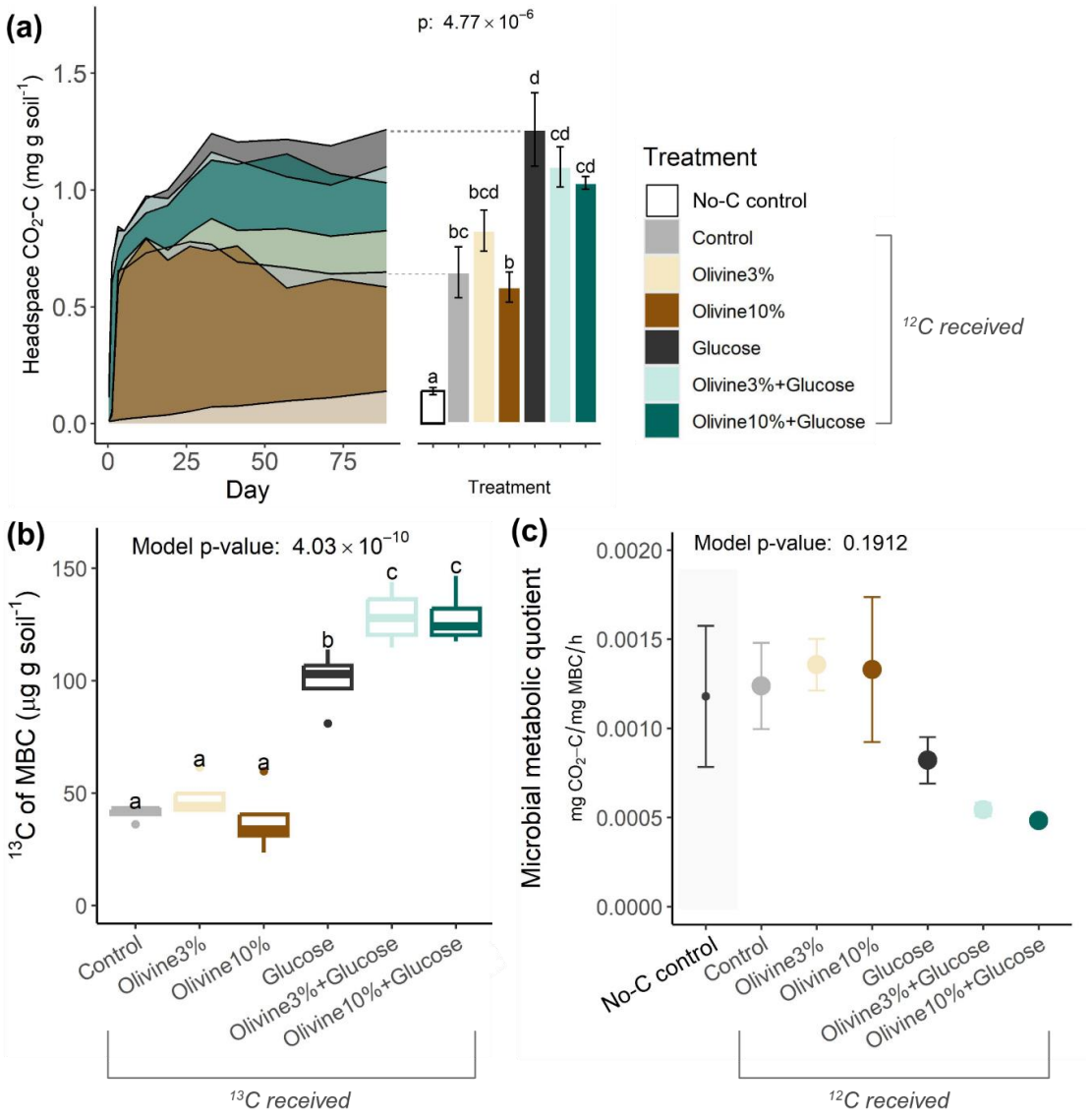

Figure 3. Microbial responses to olivine and glucose amendments during ^{13}C-labeled substrate incubation. Soils sampled at 55 weeks were sub-incubated for 12 additional weeks with a single pulse of 99% enriched ^{13}C-glucose under six treatments: a control (no olivine or glucose), Olivine3% (3% by dry mass), Olivine10% (10% by dry mass), Glucose-only (Glucose), Olivine3%+Glucose, and Olivine10%+Glucose. A parallel set of jars received unlabeled ^{12}C-glucose, and No-C controls were included to assess microbial activity. (a) Cumulative CO_2-C (mg C g^{-1} soil) in headspace over time; final values are also shown as bar graphs. (b) ^{13}C-labeled microbial biomass carbon (MBC; µg ^{13}C g^{-1} soil) as a measure of ^{13}C assimilation. (c) Microbial metabolic quotient (qCO_2; mg CO_2-C mg^{-1} MBC h^{-1}). Significant differences among treatments were determined using one-way ANOVA followed by Tukey's post hoc test ($p < 0.05$); treatments sharing the same letter are not significantly different.

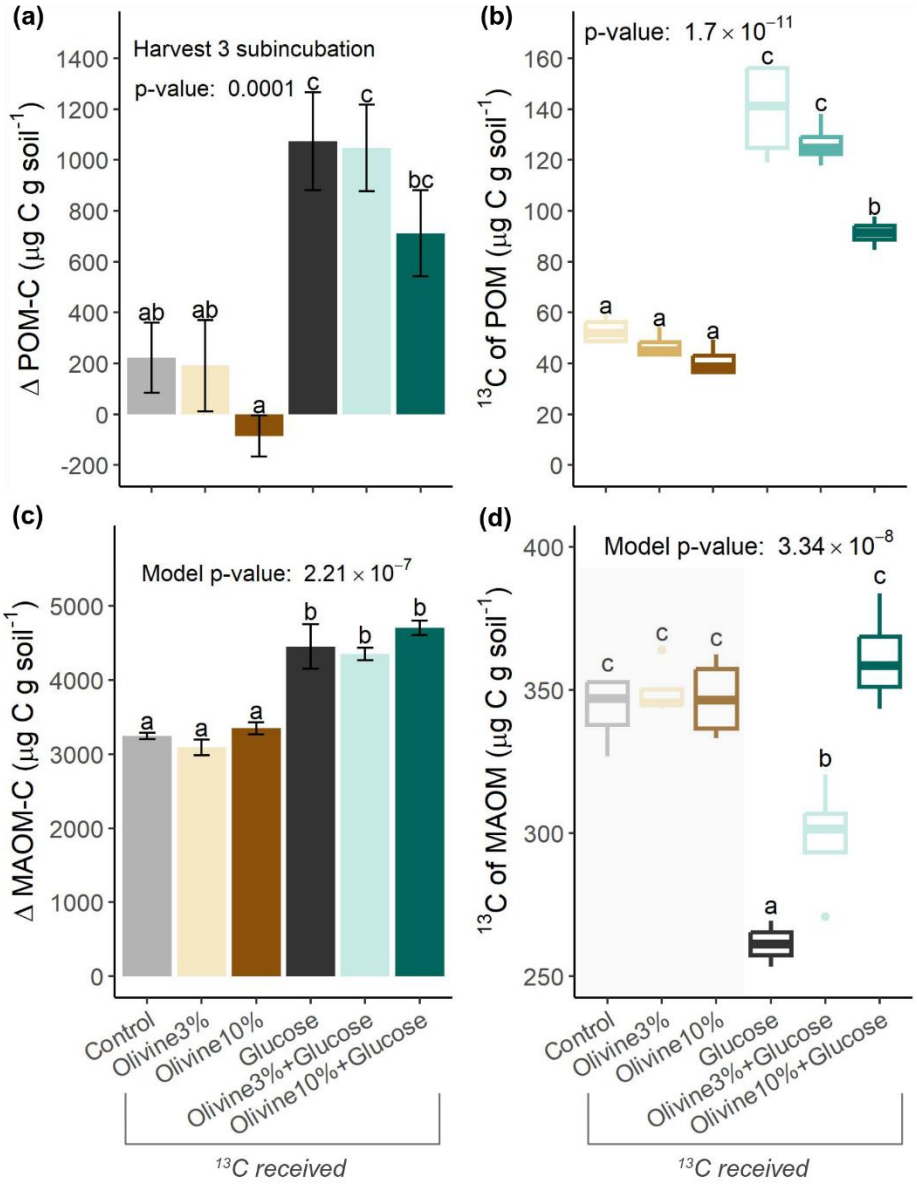

Figure 4. Soil organic carbon fraction responses to olivine and glucose amendments during ^{13}C-labeled substrate incubation. Soils sampled at 55 weeks were sub-incubated for 12 additional weeks with a single pulse of 99% enriched ^{13}C-glucose under six treatments: a control (no olivine or glucose), Olivine3% (3% by dry mass), Olivine10% (10% by dry mass), Glucose-only (Glucose), Olivine3%+Glucose, and Olivine10%+Glucose. Delta (Δ) denotes baseline-subtracted values. (a) Change in particulate organic matter carbon (ΔPOM-C; µg C g^{-1} soil). (b) ^{13}C-POM (µg ^{13}C g^{-1} soil). (c) Change in mineral-associated organic matter carbon (ΔMAOM-C; µg C g^{-1} soil). (d) ^{13}C-MAOM (µg ^{13}C g^{-1} soil). One-way ANOVA followed by Tukey's post hoc test ($p < 0.05$) was used to evaluate treatment effects. Treatments sharing the same letter are not significantly different.

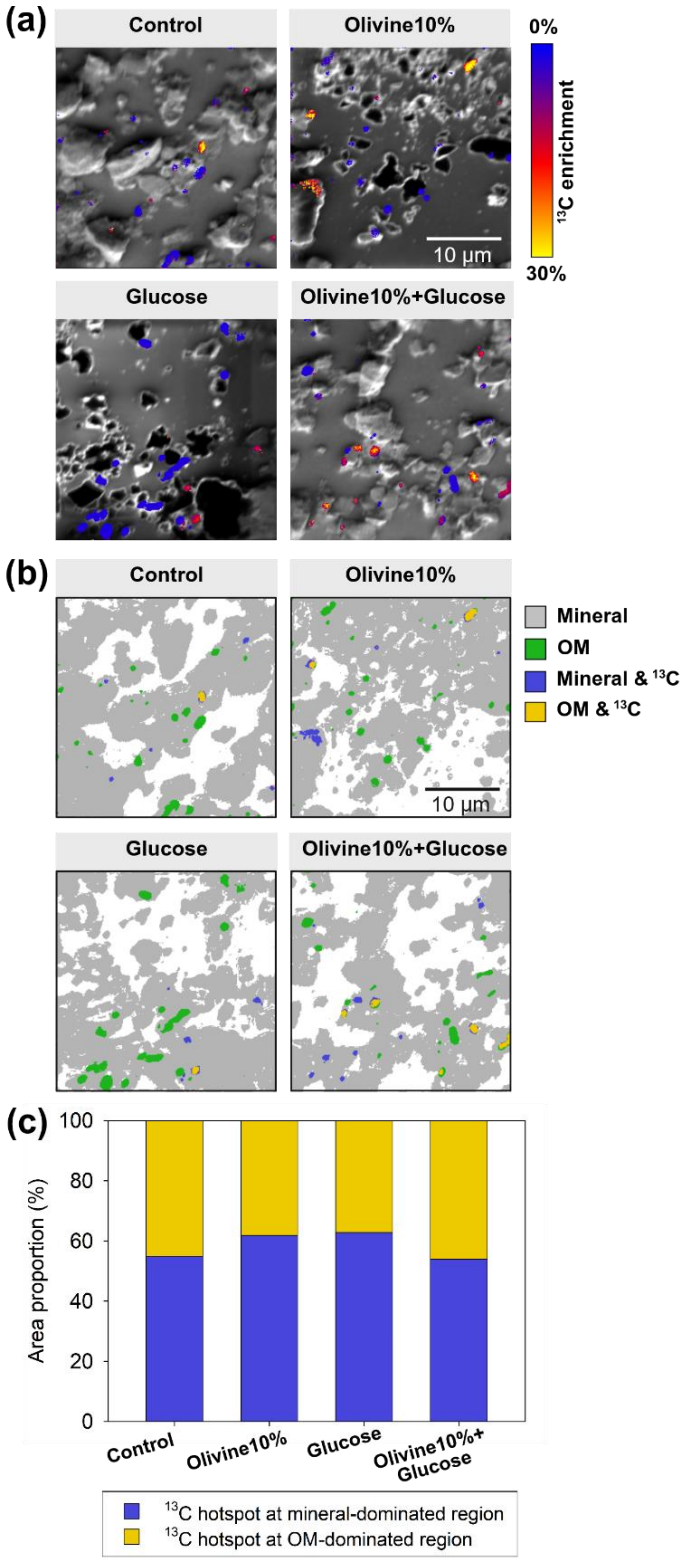

Figure 5. Microscale spatial analysis of ^{13}C allocation to MAOM after 55-weeks of weathering with NanoSIMS. NanoSIMS analysis was conducted on MAOM fractions from four treatments—control, Olivine10%, Glucose, and Olivine10%+Glucose—following a 12-week sub-incubation with 99% ^{13}C-glucose after a 55-week weathering period. The goal was to assess the spatial localization of glucose-derived ^{13}C on mineral- and OM-dominated surfaces. (a) Representative NanoSIMS images showing OM distribution and ^{13}C-enriched hotspots (heatmap, atom % ^{13}C). (b) Machine learning-based pixel classification distinguishing mineral- and OM-dominated regions, with overlaid ^{13}C hotspots. (c) Area proportion of ^{13}C hotspots associated with mineral- vs. OM-dominated regions, based on 8–31 NanoSIMS images per treatment (see Figure S4 for NanoSIMS workflow and Table S6 for the details of the full image set).

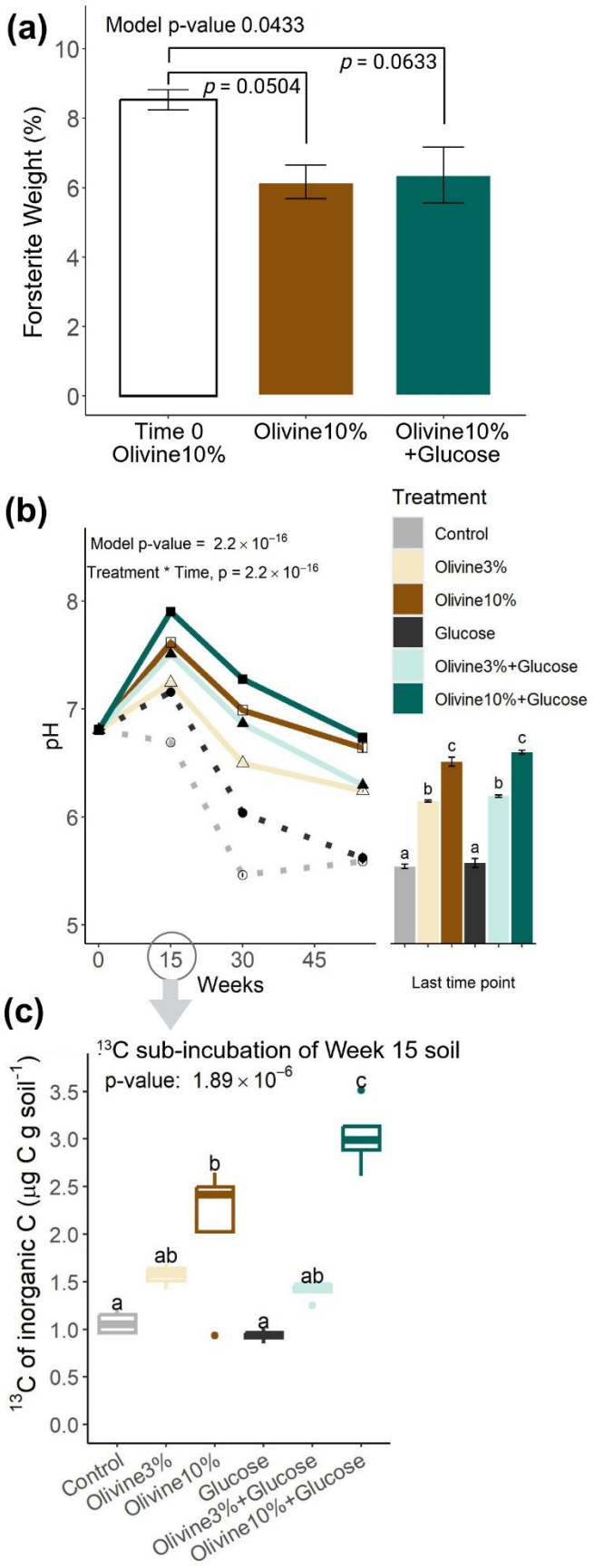

Figure 6. Changes in rock weathering indicators over a 55-week incubation. The study includes six treatments: a control (no olivine or glucose), Olivine3% (3% by dry mass), Olivine10% (10% by dry mass), Glucose-only (Glucose), Olivine3%+Glucose, and Olivine10%+Glucose. (a) Forsterite abundance determined by quantitative XRD for Olivine10% and Olivine10%+Glucose at time 0 and after 55 weeks. (b) Soil pH over time, with final data point at Week 55 shown as bar graphs. (c) ^{13}C-IC (µg ^{13}C g^{-1} soil) in soils sampled at Week 15 and sub-incubated for 12 weeks with 99% enriched ^{13}C-glucose to trace carbon allocation across six experimental conditions. Statistical significance for (b) was assessed using a linear model with treatment and time as fixed effects. Bar and box graphs for final time points indicate significant differences among treatments, determined by one-way ANOVA followed by Tukey's post hoc test ($p < 0.05$). Treatments sharing the same letter are not significantly different.

Supplementary Material

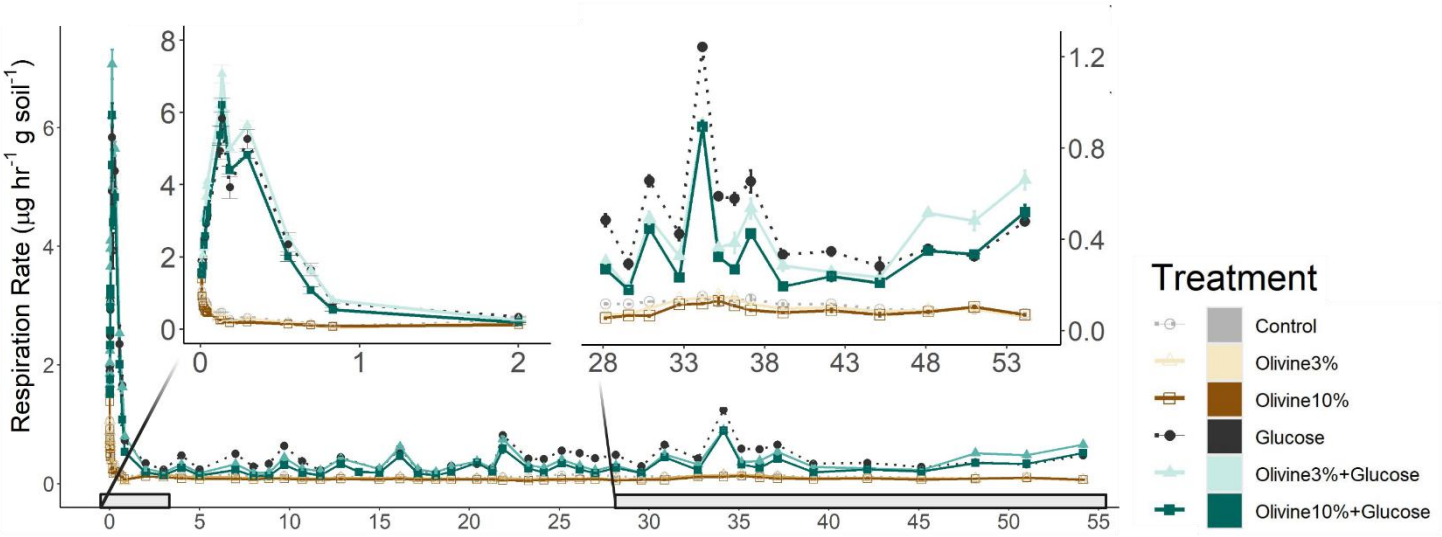

Figure S1. Changes in soil respiration rates (µg C-CO_2 hour^{-1} g soil^{-1}) over a 55-week incubation.
The study includes six treatments: a control (no olivine or glucose), Olivine3% (3% by dry mass), Olivine10% (10% by dry mass), Glucose-only (Glucose), Olivine3%+Glucose, and Olivine10%+Glucose.

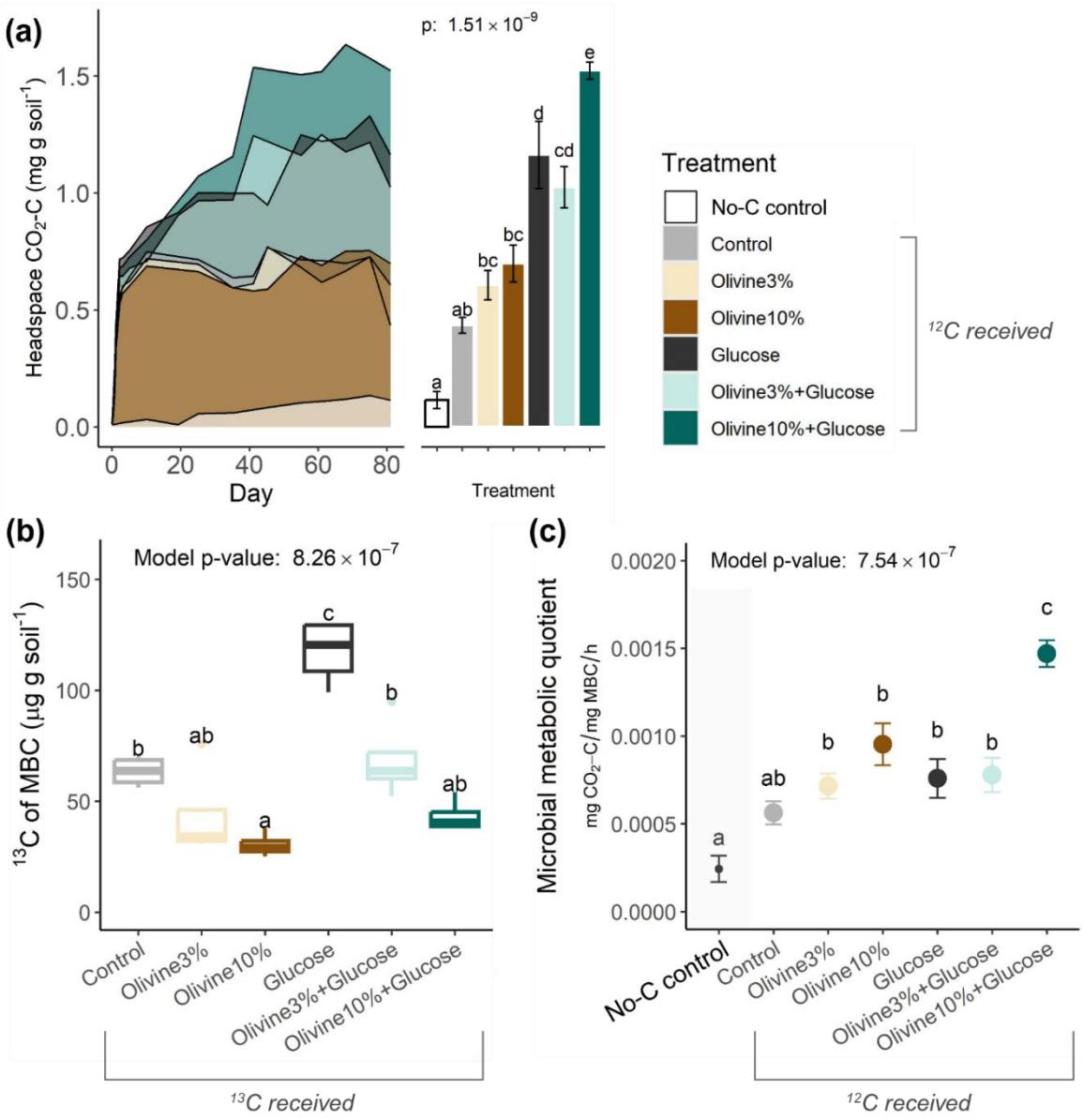

Figure S2. Microbial responses to olivine and glucose amendments during ^{13}C-labeled substrate incubation. Soils collected in Week 15 were sub-incubated for an additional 12 weeks with a single pulse of 99% enriched ^{13}C-glucose under six treatments: a control (no olivine or glucose), Olivine3% (3% by dry mass), Olivine10% (10% by dry mass), Glucose-only (Glucose), Olivine3%+Glucose, and Olivine10%+Glucose. A parallel set of jars received unlabeled ^{12}C-glucose, and No-C controls were included to assess microbial activity without ^{13}C input. (a) Cumulative CO_2-C (mg C g^{-1} soil) in headspace over time; final values are also shown as bar graphs. (b) ^{13}C-labeled microbial biomass carbon (MBC; µg ^{13}C g^{-1} soil) as a measure of ^{13}C assimilation. (c) Microbial metabolic quotient (qCO_2; mg CO_2-C mg^{-1} MBC h^{-1}). Significant differences among treatments were determined using one-way ANOVA followed by Tukey's post hoc test ($p < 0.05$); treatments sharing the same letter are not significantly different.

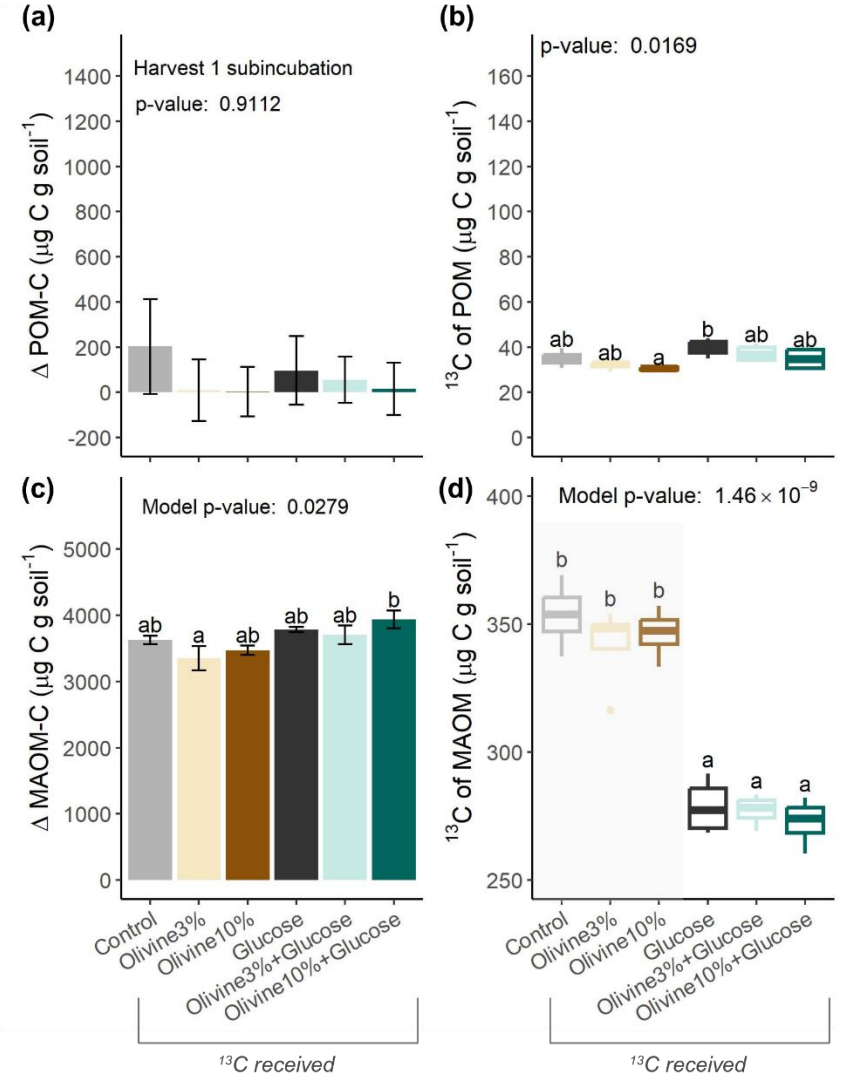

Figure S3. Soil carbon fraction responses to olivine and glucose amendments during ^{13}C-labeled substrate incubation at the early weathering stage (Week 15). Soils sampled at Week 15 were sub-incubated with 99% enriched ^{13}C-glucose to trace carbon allocation under six treatments: a control (no olivine or glucose), Olivine3% (3% by dry mass), Olivine10% (10% by dry mass), Glucose-only (Glucose), Olivine3%+Glucose, and Olivine10%+Glucose. (a) Change in particulate organic matter carbon (ΔPOM-C; µg C g^{-1} soil). (b) ^{13}C-POM (µg ^{13}C g^{-1} soil). (c) Change in mineral-associated organic matter carbon (ΔMAOM-C; µg C g^{-1} soil). (d) ^{13}C-MAOM (µg ^{13}C g^{-1} soil). One-way ANOVA followed by Tukey's post hoc test ($p < 0.05$) was used to evaluate treatment effects. Treatments sharing the same letter are not significantly different.

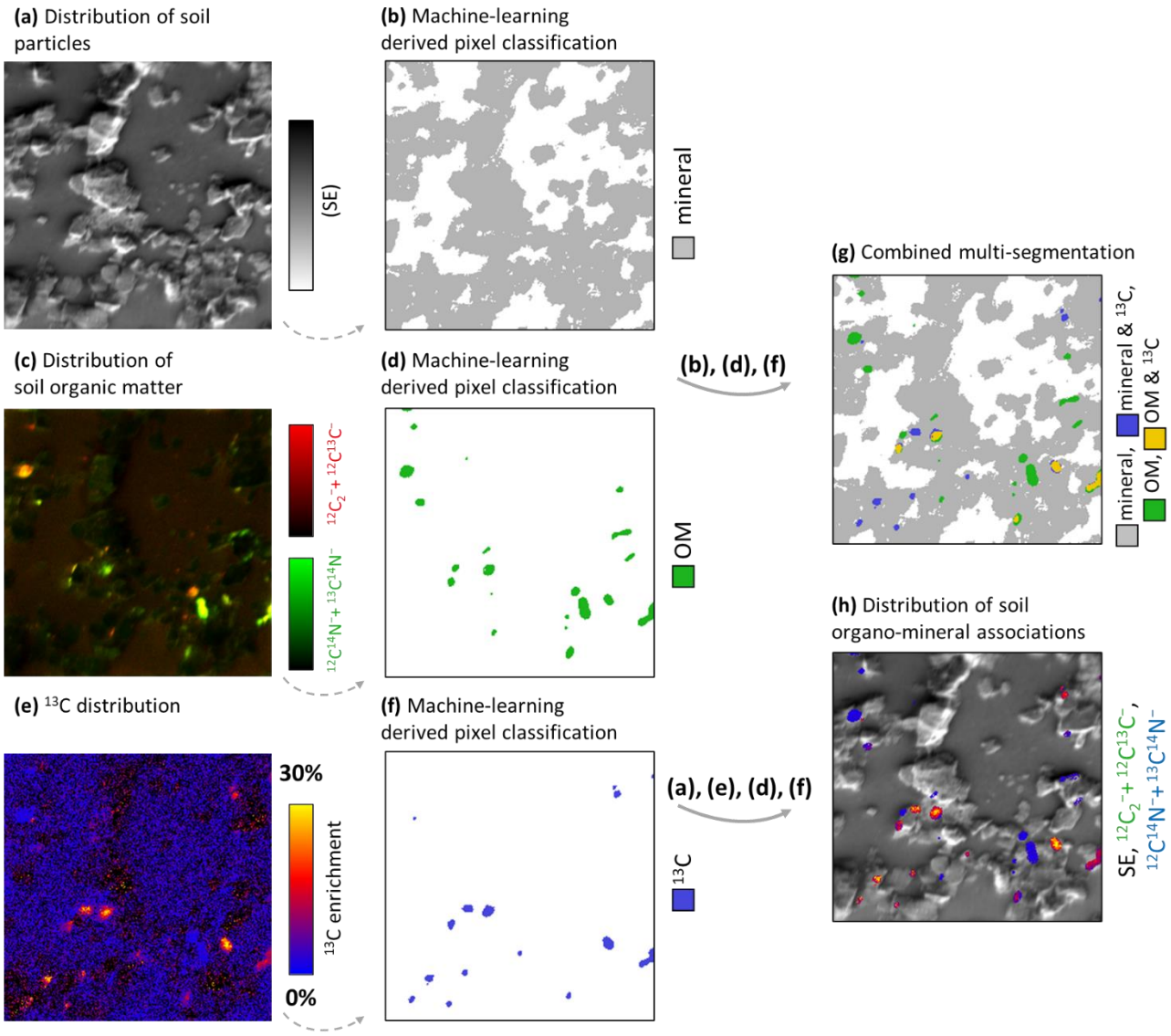

Figure S4. NanoSIMS workflow. This image analysis workflow processes different NanoSIMS channels (a, c, e) into individual segmentations based on a machine-learning algorithm (b, d, f). These segmentations are then combined to identify mineral surfaces, organic matter, and glucose-derived ^{13}C enrichment in MAOM fractions (g, h).

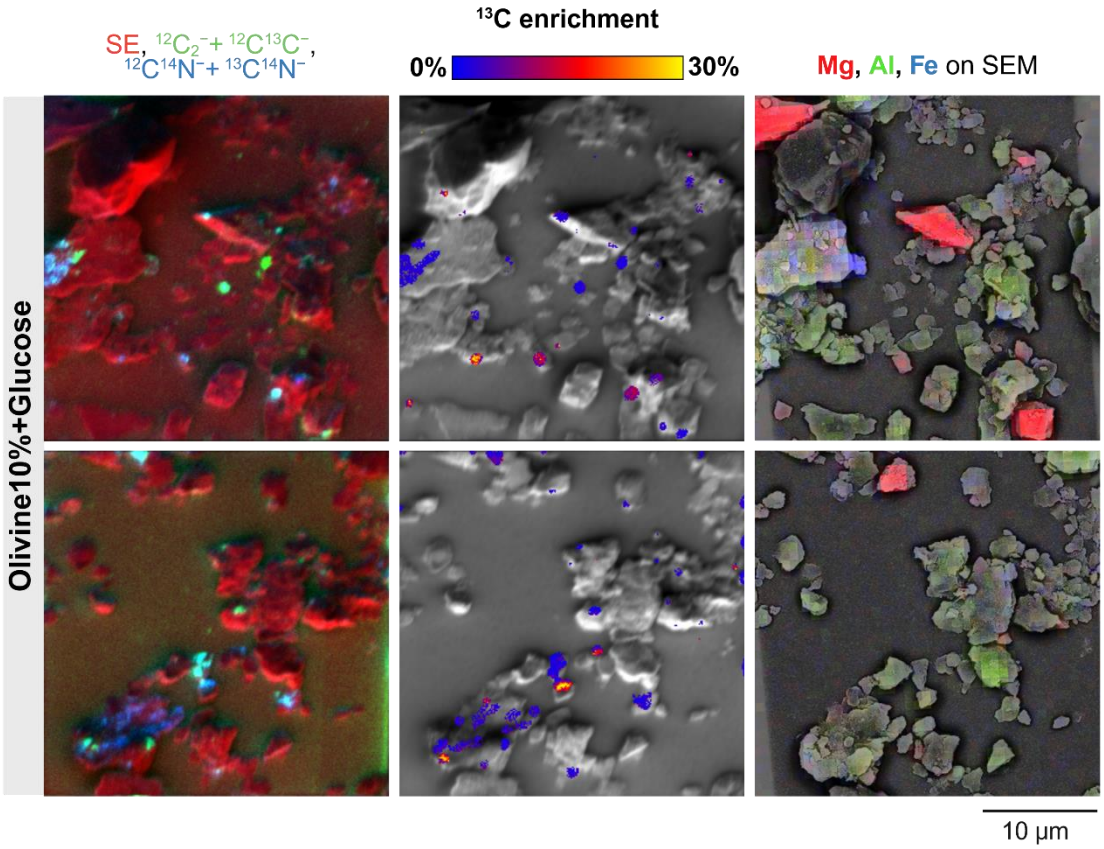

Figure S5. Co-location of organic matter (OM) patches and glucose-derived ^{13}C with Mg, Al, and Fe-distribution on the Olivine10%+Glucose treatment. Analysis on elemental and isotopic distribution was conducted on mineral-associated organic matter (MAOM) fractions from four treatments—control, Olivine10%, Glucose, and Olivine10%+Glucose—following a 12-week sub-incubation with 99% ^{13}C-glucose after a 55-week weathering period. The first column displays the spatial distribution of OM-dominated regions, characterized by higher carbon (C) and nitrogen (N) counts in MAOM fractions. The second column presents the atom % ^{13}C enrichment of ^{13}C-enriched and OM-dominated surfaces. The third row displays the distribution of magnesium (Mg), aluminum (Al), and iron (Fe) as detected by SEM-EDS.

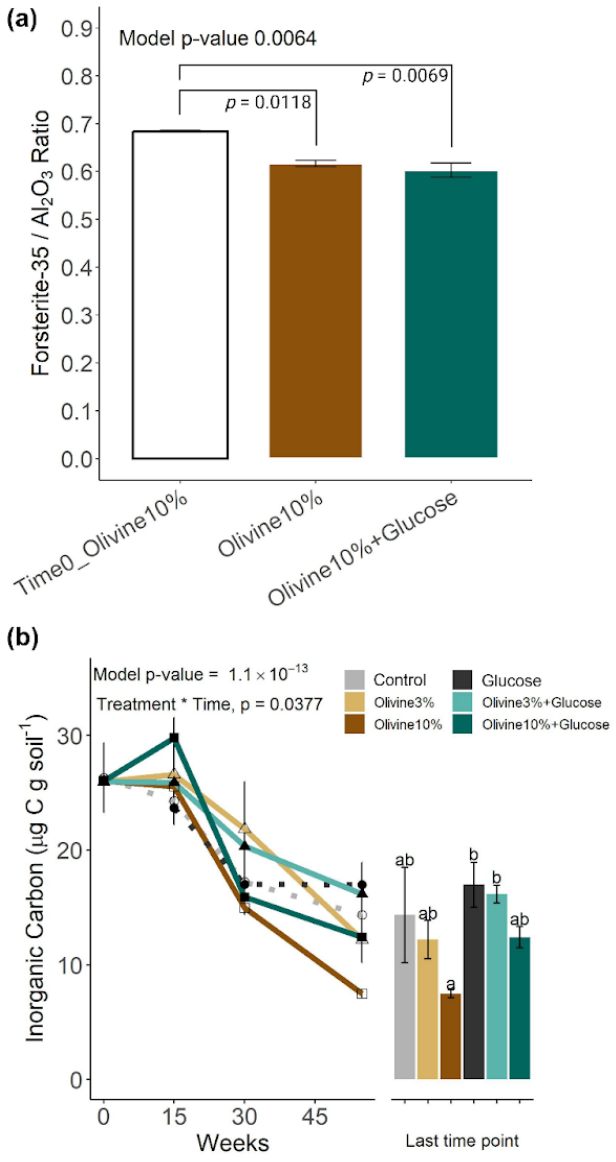

Figure S6. Changes in weathering indicators over a 55-week incubation. The study includes six treatments: a control (no olivine or glucose), Olivine3% (3% by dry mass), Olivine10% (10% by dry mass), Glucose-only (Glucose), Olivine3%+Glucose, and Olivine10%+Glucose. (a) Mineral intensity factor (MIF) for forsterite, expressed as the ratio of forsterite peak intensity to internal corundum standard (Al_2O_3), for Olivine10% and Olivine10%+Glucose treatments at time 0 and after 55 weeks. (b) Inorganic carbon (µg C g^{-1} soil) over time, with final time point data shown as bar graphs. For bar graphs, one-way ANOVA was used to evaluate treatment effects, followed by Tukey's post hoc test for pairwise comparisons ($p < 0.05$). Statistical significance for (b) was assessed using a linear model with treatment and time as fixed effects.

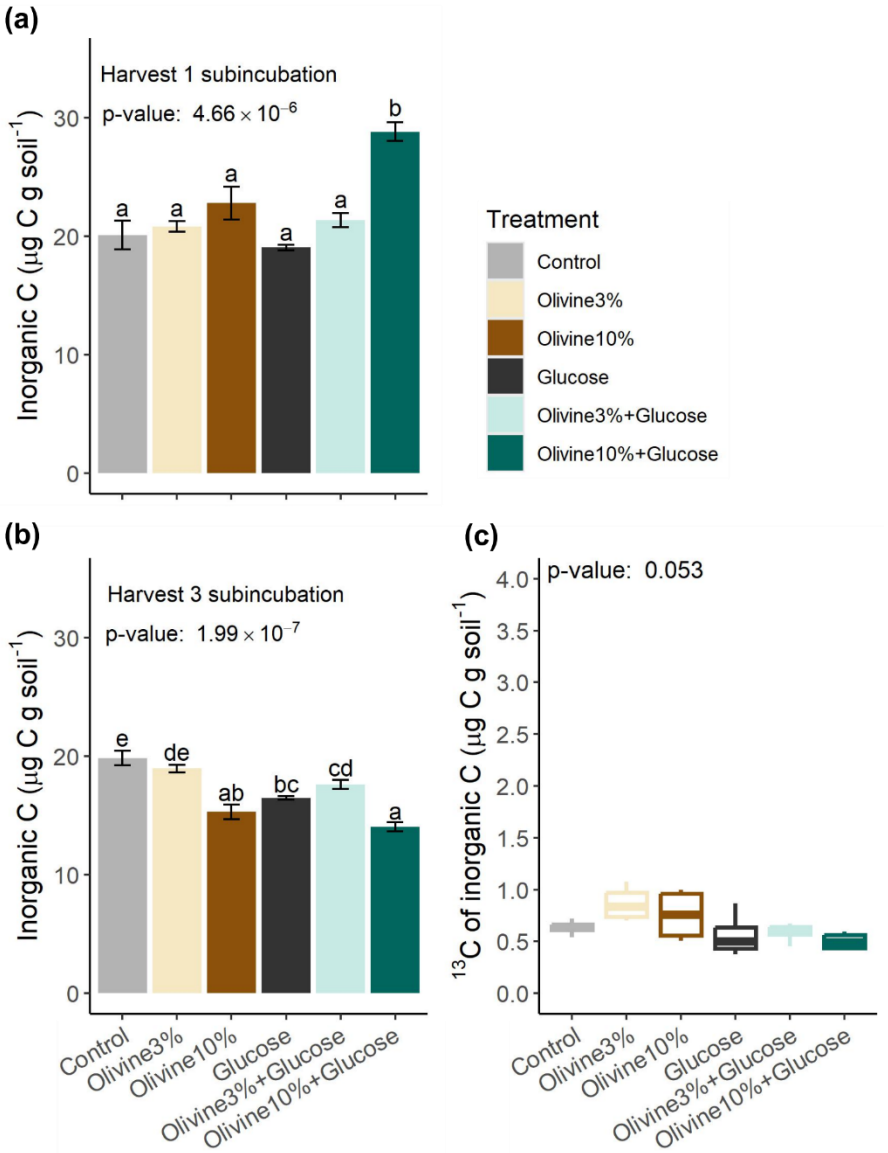

Figure S7. Inorganic carbon responses to olivine and glucose amendments during ^{13}C-labeled substrate incubation at the early (Week 15) and later (Week 55) weathering stages. Soil sampled at weeks 15 and 55 were sub-incubated with 99% enriched ^{13}C-glucose for 12-weeks to trace carbon allocation under six treatments: a control (no olivine or glucose), Olivine3% (3% by dry mass), Olivine10% (10% by dry mass), Glucose-only (Glucose), Olivine3%+Glucose, and Olivine10%+Glucose. (a) Inorganic carbon concentrations (IC; µg C g^{-1} soil) in the Week 15 soil sub-incubation. (b) IC concentrations in the Week 55 soil sub-incubation. (c) ^{13}C-IC in the Week 55 soil sub-incubation. One-way ANOVA followed by Tukey's post hoc test ($p < 0.05$) was used to evaluate treatment effects. Treatments sharing the same letter are not significantly different.

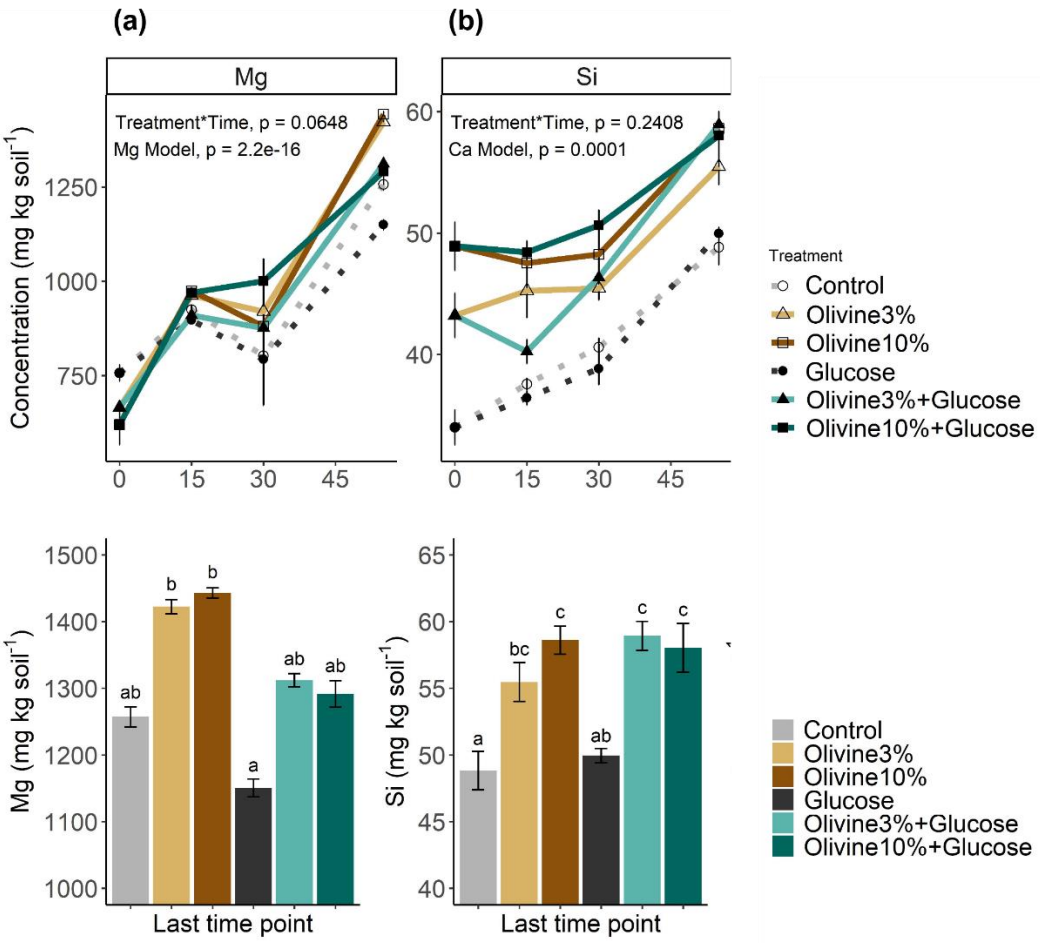

Figure S8. Changes in exchangeable cations over a 55-week incubation. Soils were incubated under six treatments: a control (no olivine or glucose), Olivine3% (3% by dry mass), Olivine10% (10% by dry mass), Glucose-only (Glucose), Olivine3%+Glucose, and Olivine10%+Glucose. Concentrations (mg kg^{-1} soil) of exchangeable cations were measured at 0, 15, 30, and 45 weeks and are shown for: (a) magnesium (Mg^{2+}) and (b) silicon (Si^{4+}). The upper line plots show temporal dynamics; bar graphs below each panel display final concentrations at Week 55. Statistical significance was assessed using linear models with treatment and time as fixed effects. For final time point comparisons, one-way ANOVA followed by Tukey's post hoc test ($p < 0.05$) was used. Treatments sharing the same letter are not significantly different.

Table S1. Mineralogical and elemental composition of the olivine amendment. Mineral phases were identified by quantitative X-ray diffraction (qXRD), with values reported as average weight percentages and standard deviations. Elemental oxide concentrations were determined by lithium metaborate/tetraborate fusion followed by inductively coupled plasma emission spectrometry (ICP-ES; method LF300). Method detection limits (MDLs) are provided for each element.

Olivine Mineral Phase	Average (%)	Standard deviation
Forsterite	85.30	1.45
Kaolinite_C1_ideal_structure_BISH	2.74	0.55
Lizardite1t	2.17	0.93
Quartz	1.76	0.39
Hornblende_iron_magnesium	1.64	0.45
Plagioclase_Albite	1.34	0.66
Gibbsite	1.27	0.26
Talc_C-1	1.18	0.38
Dolomite	0.77	0.05
Plagioclase_OligoclaseAn16	0.75	0.32
Microcline_intermediate2	0.74	0.70
Vermiculite	0.25	0.12
Plagioclase_Labradorite_An65	0.09	0.15
Weighted Total	**100**	

Element	Content (%)	Method Detection Limit (%)
MgO (%)	46.13	0.01
SiO_2 (%)	41.43	0.01
Fe_2O_3 (%)	8.34	0.04
Al_2O_3 (%)	0.57	0.01
Cr_2O_3 (%)	0.557	0.01
CaO (%)	0.21	0.01
MnO (%)	0.12	0.002
Na_2O (%)	0.06	0.01
K_2O (%)	0.04	0.01
TiO_2 (%)	0.02	0.01
P_2O_5 (%)	<0.01	0.01
BaO (%)	<0.01	0.01
LOI (%)	2.2	0.01
Sum (%)	100.07	0.5

Table S2. Particle size distribution of the crushed olivine amendment. Particle size distribution was determined using an LS-230 Particle Size Analyzer under dry and wet measurement conditions. Values represent the percentage of particles within each size range and cumulative totals.

	Dry measurement		Wet measurement	
Ranges of particle size distribution (µm)	**Within the range (%)**	**Cumulative (%)**	**Within the range (%)**	**Cumulative (%)**
0 - 2	19.00	19.00	24.69	24.69
2 - 53	64.87	83.87	61.71	86.40
53 - 100	11.92	95.79	9.91	96.31
100 - 200	4.20	99.99	3.68	99.98
200 - 2000	0.002	99.99	0.0001	99.98
Sum	**99.99**		**99.98**	

Table S3. Soil carbon fraction dynamics under six treatments—a control (no olivine or glucose), Olivine3% (3% by dry mass), Olivine10% (10% by dry mass), Glucose-only (Glucose), Olivine3%+Glucose, and Olivine10%+Glucose—across a 55-week microcosm incubation. Reported measurements include microbial biomass carbon (MBC; μg C g^{-1} soil), total carbon (mg C g^{-1} soil), mineral-associated organic matter carbon (MAOM-C; mg C g^{-1} soil), and particulate organic matter carbon (POM-C; mg C g^{-1} soil). Values are shown as mean ± standard error. MBC and total C were analyzed using linear models with treatment and time as fixed effects. MAOM-C and POM-C values at Week 0 and Week 55, as well as changes (Δ = Week 55 – Week 0), were analyzed using one-way ANOVA. F-values, degrees of freedom, p-values, and model R^2 are reported. Means sharing the same letter are not significantly different (Tukey's HSD, $p < 0.05$).

Weeks	Measurement	Control	Olivine3%	Olivine10%	Glucose	Olivine3% +Glucose	Olivine10% +Glucose	F-Value	P-Value	R^2
0	MBC (μg C g soil^{-1})	318.13 ± 2.94						*Treatment* *1200.3 (5, 63)*	*2.2×10^{-16}*	
15	MBC (μg C g soil^{-1})	319.9 ± 9.22 b	302.51 ± 2.32 ab	260.23 ± 2.96 a	660.56 ± 19.86 c	683.93 ± 20.62 c	658.28 ± 16.78 c	*Time* *147 (3, 63)*	*2.2×10^{-16}*	
30	MBC (μg C g soil^{-1})	233.78 ± 8.75 a	326.26 ± 5.14 b	266.26 ± 8.62 a	789.87 ± 40.65 c	952.6 ± 25.8 d	934.45 ± 14.69 d	*Treatment*Time* *85.68 (12, 63)*	*2.2×10^{-16}*	
55	MBC (μg C g soil^{-1})	118.94 ± 9.56 a	143.51 ± 8.91 b	117.58 ± 8.93 a	928.42 ± 9.81 c	1037.21 ± 39.69 c	1221.45 ± 36.81 d			
								373.5 (20, 63)	**2.2×10^{-16}**	**0.9916**
0	Total C (mg C g soil^{-1})	9.99 ± 0.08 b	9.65 ± 0.08 b	8.74 ± 0.26 a				*Treatment* *112.78 (5, 63)*	*2.2×10^{-16}*	
15	Total C (mg C g soil^{-1})	9.49 ± 0.24 ab	9.56 ± 0.18 ab	9.16 ± 0.12 a	10.75 ± 0.18 c	10.76 ± 0.16 c	9.97 ± 0.12 b	*Time* *58.22 (3, 63)*	*2.2×10^{-16}*	
30	Total C (mg C g soil^{-1})	9.63 ± 0.1 ab	9.66 ± 0.15 ab	9.09 ± 0.16 a	11.3 ± 0.17 c	10.92 ± 0.11 c	10.08 ± 0.07 b	*Treatment*Time* *7.2 (12, 63)*	*4.6×10^{-8}*	
55	Total C (mg C g soil^{-1})	8.46 ± 0.12 b	8.33 ± 0.09 b	7.38 ± 0.12 a	10.21 ± 0.06 c	10.61 ± 0.18 c	10.18 ± 0.17 c			
								41.25 (20, 63)	**2.2×10^{-16}**	**0.929**
0	MAOM-C (mg C g soil^{-1})	5.21 ± 0.03 b	5.14 ± 0.08 b	4.51 ± 0.06 a				38.9 (2, 9)	3.72×10^{-5}	0.8963
55	MAOM-C (mg C g soil^{-1})	5.24 ± 0.07 b	4.96 ± 0.06 ab	4.52 ± 0.15 a	6.86 ± 0.02 c	6.7 ± 0.14 c	6.47 ± 0.09 c	101.7 (5, 18)	1.50×10^{-12}	0.9658
change	Δ MAOM-C (mg C g soil^{-1})	0.04 ± 0.09 a	-0.18 ± 0.13 a	0.01 ± 0.13 a	1.65 ± 0.05 b	1.56 ± 0.19 b	1.97 ± 0.15 b	55.5 (5, 18)	2.62×10^{-10}	0.9391
0	POM-C (mg C g soil^{-1})	1.84 ± 0.1 a	1.83 ± 0.09 a	1.73 ± 0.08 a				0.27 (2, 9)	0.7688	0.0568
55	POM-C (mg C g soil^{-1})	1.33 ± 0.03 a	1.28 ± 0.08 a	1.13 ± 0.07 a	1.89 ± 0.06 b	1.68 ± 0.08 b	1.67 ± 0.09 b	16.83 (5, 18)	3.12×10^{-6}	0.8238
change	Δ POM-C (mg C g soil^{-1})	-0.51 ± 0.16 ab	-0.55 ± 0.13 a	-0.61 ± 0.11 a	0.06 ± 0.1 b	-0.15 ± 0.1 ab	-0.06 ± 0.16 ab	4.91 (5, 18)	0.0052	0.5769

Table S4. Carbon pool allocation from ^{13}C-glucose tracing in week 15 and 55 soils under seven treatments: No-C control, a control (no olivine or glucose), Olivine3% (3% by dry mass), Olivine10% (10% by dry mass), Glucose-only (Glucose), Olivine3%+Glucose, and Olivine10%+Glucose. Microbial biomass carbon (MBC; μg C g^{-1} soil) and headspace CO_2 (mg C g^{-1} soil) were measured from unlabeled (^{12}C-matching) sets. Following 12-week sub-incubations with 99% enriched ^{13}C-glucose, concentrations and tracer-derived ^{13}C content were quantified for four carbon fraction: microbial biomass carbon (MBC), inorganic carbon (IC), mineral-associated organic matter (MAOM), and particulate organic matter (POM). All fractions are reported in μg C g^{-1} soil. For each timepoint, treatment effects were assessed using one-way ANOVA followed by Tukey's post hoc test ($p < 0.05$). F-values, degrees of freedom, p-values, and model R^2 values are reported. Treatments sharing the same letter are not significantly different.

Measurement	No-C control	Control	Olivine3%	Olivine10%	Glucose	Olivine3% +Glucose	Olivine10% +Glucose	F-Value	P-Value	R^2
^{13}C-probing on 15 week soils										
MBC (μg C g soil^{-1})	242.84 ± 8.16 a	403.59 ± 20.77 b	435.57 ± 3.02 b	378.45 ± 8.79 b	797.06 ± 32.9 e	678.84 ± 18.85 d	535.64 ± 18.31 c	106.76 (6, 21)	1.25×10^{-14}	0.9683
Headspace CO_2 (mg C g soil^{-1})	0.11 ± 0.04 a	0.43 ± 0.03 ab	0.61 ± 0.06 bc	0.7 ± 0.08 bc	1.16 ± 0.14 d	1.02 ± 0.12 cd	1.52 ± 0.04 e	37.56 (6, 19)	1.51×10^{-9}	0.9222
^{13}C-MBC (μg C g soil^{-1})		63.43 ± 3.35 b	43.81 ± 10.69 ab	30.26 ± 2.7 a	117.62 ± 7.48 c	68.65 ± 9.19 b	43.38 ± 3.66 ab	20.18 (5, 18)	8.26×10^{-7}	0.8486
Inorganic Carbon (μg C g soil^{-1})		20.11 ± 1.21 a	20.84 ± 0.44 a	22.81 ± 1.39 a	19.05 ± 0.23 a	21.39 ± 0.6 a	28.84 ± 0.78 b	15.91 (5, 18)	4.66×10^{-6}	0.8155
^{13}C-IC (μg C g soil^{-1})		1.06 ± 0.06 a	1.57 ± 0.06 ab	2.11 ± 0.39 b	0.93 ± 0.03 a	1.41 ± 0.05 ab	3.03 ± 0.19 c	18.04 (5, 18)	1.89×10^{-6}	0.8336
MAOM (μg C g soil^{-1})		8831.21 ± 68.6 cd	8490.13 ± 138.58 bc	7976.71 ± 52.43 a	8989.08 ± 5.14 d	8842.99 ± 68.4 cd	8444.69 ± 80.44 b	21.84 (5, 18)	4.58×10^{-7}	0.8585
^{13}C-MAOM (μg C g soil^{-1})		353.57 ± 6.64 b	341.74 ± 8.55 b	346.33 ± 4.98 b	278.71 ± 5.48 a	277.25 ± 3.11 a	272.66 ± 4.68 a	45.12 (5, 18)	1.46×10^{-9}	0.9261
POM (μg C g soil^{-1})		2040.97 ± 95.96 b	1835.18 ± 46.02 ab	1737.08 ± 36.58 a	1934.26 ± 23.33 ab	1880.35 ± 29.91 ab	1749.87 ± 100.41 a	3.30 (5, 18)	0.02742	0.4782
^{13}C-POM (μg C g soil^{-1})		34.9 ± 1.83 ab	31.89 ± 0.96 ab	30.45 ± 0.59 a	39.76 ± 1.98 b	37.23 ± 1.91 ab	34.77 ± 2.53 ab	3.74 (5, 18)	0.01694	0.5096
^{13}C-probing on 55 week soils										
MBC (μg C g soil^{-1})	67.15 ± 11.96 a	256.9 ± 11.07 b	316.18 ± 33.74 b	236.13 ± 45.19 b	738.26 ± 33.25 c	992.68 ± 52.49 d	1004.33 ± 35.91 d	122.4 (6, 21)	3.14×10^{-15}	0.9722
Headspace CO_2 (mg C g soil^{-1})	0.14 ± 0.02 a	0.65 ± 0.13 bc	0.83 ± 0.12 bcd	0.58 ± 0.07 b	1.26 ± 0.18 d	1.1 ± 0.1 cd	1.03 ± 0.03 cd	17.84 (6, 15)	4.77×10^{-6}	0.8771
^{13}C-MBC (μg C g soil^{-1})		40.87 ± 1.6 a	47.98 ± 4.54 a	37.67 ± 7.76 a	100.18 ± 6.94 b	128.64 ± 6.41 c	128.11 ± 6.49 c	52.7 (5, 18)	4.03×10^{-10}	0.9361

Inorganic Carbon ($\mu g\ C\ g\ soil^{-1}$)	19.86 ± 0.62 e	18.97 ± 0.31 de	15.31 ± 0.63 ab	16.49 ± 0.16 bc	17.61 ± 0.38 cd	14.04 ± 0.39 a	24.52 (5, 18)	1.99×10^{-7}	0.872
^{13}C-IC ($\mu g\ C\ g\ soil^{-1}$)	0.63 ± 0.04	0.86 ± 0.09	0.75 ± 0.13	0.56 ± 0.11	0.59 ± 0.05	0.5 ± 0.04	2.72 (5, 18)	0.053	0.4303
MAOM ($\mu g\ C\ g\ soil^{-1}$)	8453.66 ± 56.81 a	8228.6 ± 73.56 a	7856.75 ± 137.77 a	9657.82 ± 315.32 b	9489.98 ± 22.57 b	9212.33 ± 106.35 b	23.47 (5, 18)	2.65×10^{-7}	0.867
^{13}C-MAOM ($\mu g\ C\ g\ soil^{-1}$)	343.6 ± 6.2 c	349.67 ± 4.85 c	347.2 ± 7.01 c	250.02 ± 8.02 a	298.52 ± 10.3 b	361.1 ± 8.6 c	30.64 (5, 18)	3.34×10^{-8}	0.8949
POM ($\mu g\ C\ g\ soil^{-1}$)	2060.18 ± 51.59 ab	2016.5 ± 88.46 ab	1649.02 ± 30.64 a	2911.72 ± 183.13 c	2872.69 ± 148.9 c	2445.73 ± 106.85 bc	19.57 (5, 18)	1.04×10^{-6}	0.8446
^{13}C-POM ($\mu g\ C\ g\ soil^{-1}$)	52.87 ± 2.6 a	46.73 ± 2.63 a	40.83 ± 2.98 a	139.59 ± 9.75 c	126.37 ± 4.24 c	91.28 ± 2.76 b	76.71 (5, 18)	1.70×10^{-11}	0.9552

Table S5. Weathering indicator dynamics over a 55-week incubation under six treatments: a control (no olivine or glucose), Olivine3% (3% by dry mass), Olivine10% (10% by dry mass), Glucose-only (Glucose), Olivine3%+Glucose, and Olivine10%+Glucose. Reported variables include soil pH, inorganic carbon (IC; μg C g^{-1} soil), exchangeable magnesium (Mg; mg kg^{-1} soil), and exchangeable silicon (Si; mg kg^{-1} soil). Data were analyzed using linear models with treatment and time as fixed effects. Treatment differences at each time point were evaluated using one-way ANOVA followed by Tukey's post hoc test ($p < 0.05$). Treatments sharing the same letter are not significantly different.

Weeks	Measurement	Control	Olivine3%	Olivine10%	Glucose	Olivine3% +Glucose	Olivine10% +Glucose	F-Value	P-Value	R^2
0	pH	6.8 ± 0.01						*Treatment 1203.82 (5, 63)*	*2.2×10^{-16}*	
15	pH	6.69 ± 0.03 a	7.24 ± 0.01 b	7.62 ± 0.03 d	7.16 ± 0.02 b	7.51 ± 0.04 c	7.9 ± 0.01 e	*Time 2629.06 (3, 63)*	*2.2×10^{-16}*	
30	pH	5.46 ± 0.02 a	6.5 ± 0.03 c	6.99 ± 0.02 e	6.04 ± 0.01 b	6.86 ± 0.01 d	7.28 ± 0.02 f	*Treatment*Time 121.12 (12, 63)*	*2.2×10^{-16}*	
55	pH	5.59 ± 0.02 a	6.24 ± 0.01 b	6.64 ± 0.04 c	5.62 ± 0.05 a	6.3 ± 0.01 b	6.74 ± 0.02 c			
								768 (20, 63)	**2.2×10^{-16}**	**0.9959**
0	IC (μg C g $soil^{-1}$)	26.28 ± 2.15	25.95 ± 0.33	26.03 ± 1.18				*Treatment 1.52 (5, 63)*	*0.195*	
15	IC (μg C g $soil^{-1}$)	24.27 ± 1.14	26.58 ± 1.71	25.52 ± 1.02	23.66 ± 1.47	25.89 ± 0.95	29.76 ± 1.79	*Time 62.36 (3, 63)*	*2.2×10^{-16}*	
30	IC (μg C g $soil^{-1}$)	17.19 ± 0.43	21.82 ± 4.09	14.95 ± 0.56	17.02 ± 1.43	20.31 ± 1.86	15.9 ± 0.73	*Treatment*Time 2.01 (12, 63)*	*0.03774*	
55	IC (μg C g $soil^{-1}$)	14.33 ± 4.16 ab	12.19 ± 1.67 ab	7.47 ± 0.33 a	16.96 ± 1.98 b	16.16 ± 0.77 b	12.41 ± 0.93 ab			
								10.94 (20, 63)	**1.10×10^{-13}**	**0.7765**
0	Mg (mg kg $soil^{-1}$)	830.25 ± 29.56	664.88 ± 7.36	620.05 ± 53.88				*Treatment 3.79 (5, 62)*	*0.004629*	
15	Mg (mg kg $soil^{-1}$)	924.44 ± 12.06	962.72 ± 8.84	974.71 ± 7.43	897.35 ± 5.12	909.84 ± 22.51	969.88 ± 14.4	*Time 124.06 (3, 62)*	*2.2×10^{-16}*	
30	Mg (mg kg $soil^{-1}$)	802.72 ± 68.59	919.93 ± 80.93	880.04 ± 111.94	793.04 ± 122.51	876.02 ± 86.89	1000.69 ± 59.02	*Treatment*Time 1.82 (12, 62)*	*0.064849*	
55	Mg (mg kg $soil^{-1}$)	1257.23 ± 15.06 ab	1422.53 ± 10.56 b	1443.09 ± 7.7 b	1150.57 ± 13.31 a	1312.11 ± 9.92 ab	1291.69 ± 19.86 ab			
								20.65 (20, 62)	**2.2×10^{-16}**	**0.8695**
0	Si (mg kg $soil^{-1}$)	34.21 ± 0.67 a	43.21 ± 1.83 b	48.93 ± 1.98 c				*Treatment 44.23 (5, 62)*	*2.2×10^{-16}*	
15	Si (mg kg $soil^{-1}$)	37.54 ± 0.51 a	45.25 ± 2.24 bc	47.51 ± 0.95 c	36.42 ± 0.6 a	40.24 ± 1 ab	48.41 ± 0.97 c	*Time 108.3 (3, 62)*	*2.2×10^{-16}*	
30	Si (mg kg $soil^{-1}$)	40.6 ± 0.74 ab	45.44 ± 0.95 bc	48.23 ± 1.63 c	38.81 ± 1.33 a	46.35 ± 1.32 c	50.64 ± 1.28 c	*Treatment*Time 2.06 (12, 62)*	*0.03298*	
55	Si (mg kg $soil^{-1}$)	48.83 ± 1.45 a	55.48 ± 1.46 bc	58.62 ± 1.06 c	49.95 ± 0.53 ab	58.93 ± 1.09 c	58.04 ± 1.82 c			

			28.54 (20, 62)	**2.2×10^{-16}**	**0.902**

Table S6. Summary of NanoSIMS image analysis for MAOM fractions across four treatments—Control, Olivine10%, Glucose, and Olivine10%+Glucose—following a 12-week sub-incubation with 99% enriched ^{13}C-glucose after 55-weeks of weathering. For each treatment, total particle area, organic matter (OM)-dominated area, and ^{13}C hotspot area (µm²) were quantified across NanoSIMS images using machine learning-based pixel classification.

Treatments	Particle area (µm^2)	OM-dominated area (µm^2)	^{13}C hotspot area (µm^2)
Control	18882.4	649.8	142.9
Olivine10%	9499.4	878.9	46.3
Glucose	4517.0	175.8	14.7
Olivine10%+Glucose	14624.8	642.2	141.1